Journal of Medicinal Chemistry

pubs.acs.org/jmc

Article

Defining Target Engagement Required for Efficacy *In Vivo* at the Retinoic Acid Receptor-Related Orphan Receptor C2 (RORγt)

Charles W. Lugar,* Christian A. Clarke, Richard Morphy, Helene Rudyk, Selma Sapmaz, Ryan E. Stites, Grant M. Vaught, Kelly Furness, Howard B. Broughton, Greg L. Durst, David K. Clawson, Stephanie L. Stout, Sherry Y. Guo, Jim D. Durbin, Keith R. Stayrook, Denise D. Edmondson, Kristy Kikly, Nicole E. New, Holly A. Bina, Mark G. Chambers, Pamela Shetler, William Y. Chang, Veavi Ching-Yun Chang, Rob Barr, Wendy H. Gough, Jimmy P. Steele, Brian Getman, Nita Patel, Brian M. Mathes, and Timothy I. Richardson

Cite This: *J. Med. Chem.* 2021, 64, 5470−5484

Read Online

ACCESS | Metrics & More | Article Recommendations | Supporting Information

ABSTRACT: The Th17 pathway has been implicated in autoimmune diseases. The retinoic acid receptor-related orphan receptor C2 (RORγt) is a master regulator of Th17 cells and controls the expression of IL-17A. RORγt is expressed primarily in IL-17A-producing lymphoid cells. Here we describe a virtual screen of the ligand-binding pocket and subsequent screen in a binding assay that identified the 1-benzyl-4′,5′-dihydrospiro[piperidine-4,7′-thieno[2,3-*c*]pyran]-2′-carboxamide scaffold as a starting point for optimization of binding affinity and functional activity guided by structure-based design. Compound **12** demonstrated activity in a mouse PK/PD model and efficacy in an inflammatory arthritis mouse model that were used to define the level and duration of target engagement required for efficacy *in vivo*. Further optimization to improve ADME and physicochemical properties with guidance from simulations and modeling provided compound **22**, which is projected to achieve the level and duration of target engagement required for efficacy in the clinic.

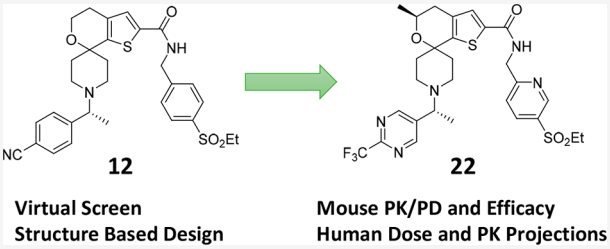

INTRODUCTION

There are over 80 described autoimmune diseases affecting approximately 10% of the population.[1] Antibodies to proinflammatory cytokines such as tumor necrosis factor α (TNFα) have become important therapeutics for many autoimmune diseases including rheumatoid arthritis, psoriasis, psoriatic arthritis, and inflammatory bowel diseases. More recently antibodies targeting the cytokine interleukin-17A (IL-17A) have shown superior efficacy for the treatment of psoriasis, while targeting interleukin-23 (IL-23) delivers similar efficacy with the potential for a longer duration of remission.[2] IL-17A is produced by Th17 cells, which are stabilized by IL-23 signaling. Other IL-17A producing cells include natural killer (NK) T cells, NK cells, myeloid cells, and innate lymphoid cells (ILC3).[3] New targets within the IL-17A/IL-23 signaling networks (the Th17 pathway) offer significant opportunities to improve efficacy, safety, and convenience for patients and providers.

The nuclear receptors (NRs) are a family of ligand-dependent transcription factors that respond to steroid and thyroid hormones, lipid and cholesterol metabolites, and lyophilic vitamins.[4] The retinoic acid receptor-related orphan receptor (ROR) subfamily consists of RORα, RORβ, and RORγ. The RORs have a typical NR protein architecture with a relatively small N-terminal, ligand-independent activation function 1 (AF-1) domain, a DNA binding domain (DBD), a hinge region, and a C-terminal, ligand-dependent activation 2 (AF-2) domain. In general, the RORs display constitutive functional activity and have been shown to bind a range of ligands including oxysterols[5] and cholesterol metabolites.[6] RORs bind genomic DNA as monomers to ROR response elements (ROREs), typically TAA/TNTGGTCA sequences, in the promoter regions of ROR response genes (i.e., IL17A and IL23R). When bound to DNA, the RORs recruit co-regulators that either activate or suppress transcription. Gene expression is regulated positively or negatively depending on the ligand bound in the LBD, the chromatin context, the cell type, and state of the cell.

The RORC gene codes for two splice variants giving rise to isoforms γ1 and γ2, the latter most commonly referred to as RORγt, which is expressed primarily in IL-17A-producing cells

Received: November 5, 2020
Published: April 14, 2021

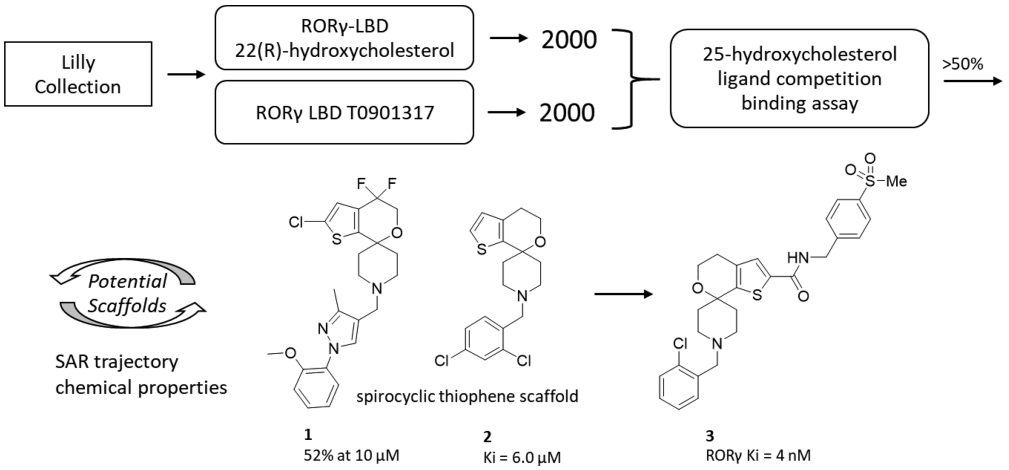

Figure 1. Discovery and evolution of 4′,5′-dihydrospiro[piperidine-4,7′-thieno[2,3-*c*]pyran] RORγ inhibitors. The Lilly compound collection was screened through two virtual models. Two sets of compounds, 2000 each, predicted to have high affinity were selected for the competitive binding assay using radio-labeled [^{3}H]-25-hydroxycholesterol and the LBD of human RORγ (309−508). Compounds with >50% inhibition of binding at 10 μM and favorable cLogP were selected for further evaluation as potential scaffolds. The spirocyclic thiophene scaffold was selected and elaborated into compound **3**.

of the immune system. The two splice variants produce identical proteins except for an additional 20 amino acids at the N-terminus of the AF1 domain in RORγ. To date, no functional distinction has been attributed to these two distinct protein isoforms beyond their tissue specific expression. RORγt expression is restricted to IL-17A-producing lymphoid cells, while RORγ is more widely expressed especially in liver, muscle, adipose, and kidney tissues.[7]

RORγt, in response to T cell receptor activation and IL-23/IL-23R receptor signaling, is required for the differentiation and maintenance of naive CD4$^+$ T cells into a subset of T cells designated Th17, which are distinct from the classical Th1 and Th2 cells. Th17 cells produce IL-17A and IL-17F in addition to a range of other factors known to drive inflammatory responses, including IL-26, GM-CSF, CXCL1, and CCL20. NK cells and innate lymphoid cells such as lymphoid tissue inducer (LTi)-like cells also express IL-23 receptor and RORγt and produce IL-17A in response to various stimuli and IL-23. There is substantial genetic and correlative evidence that IL-23-responsive, RORγt, and IL-17A-expressing cells are etiologically associated with autoimmune diseases such as psoriasis,[8] psoriatic arthritis,[9] and ankylosing spondylitis.[10] Humans with a homozygous loss-of-function mutation in the RORC gene lack IL-17 producing cells.[11] Thus, targeted inhibition of RORγt may be an important clinical strategy for reducing the pathogenesis of immunological diseases because it would inhibit the activation and differentiation of RORγt-dependent, IL-17A-producing lymphoid cells.[12]

Thymic lymphomas have been observed in mice with complete ablation of RORC expression; however, lymphomas have not been observed in heterozygous knockouts or conditional knockouts with incomplete gene deletion.[13] One case of thymic cortical hyperplasia, which can be interpreted as a preneoplastic feature, has been reported in a single rat after 13 weeks of administration of a small-molecule inhibitor of RORγ.[14] To date, however, the development of thymic T cell lymphomas has not been reported in humans with a homozygous loss-of-function mutation in the RORC gene.[11] The theoretical risk of chronic administration of RORγ inhibitors will require further evaluation in chronic and carcinogenicity toxicology studies.

Various endogenous and synthetic RORγ ligands have been identified and designed that modulate RORγ transcriptional activity.[15] Here we describe efforts that identified the 1-benzyl-4′,5′-dihydrospiro[piperidine-4,7′-thieno[2,3-*c*]pyran]-2′-carboxamide scaffold as a starting point for potent and selective ligands that were optimized and used to define the level and duration of target engagement required for efficacy *in vivo*. We also describe physiologically-based pharmacokinetic (PBPK) modeling that was used to project doses of compound **22** and human PK parameters expected to provide efficacy in the clinic.

RESULTS

Virtual Screen. The ligand-binding pocket of RORγ is large and predominantly hydrophobic (575 Å^3, 61% of total cavity volume).[16] We expected a high-throughput screen (HTS) would result in a high hit rate, returning many hydrophobic molecules that would be difficult to optimize. Therefore, rather than an HTS, we opted for an *in silico* screen of the Lilly collection, which allowed us to greatly diminish the number of compounds assayed and allowed us to prioritize compounds with drug-like properties for testing;[17] see Figure 1. A docking model was constructed using the co-crystal structure 22(*R*)-hydroxycholesterol bound in the LBD of RORγ (PDB 3L0J).[18] We selected 2000 compounds predicted to have a high binding affinity. A second virtual screen was run using a docking model based on T0901317 bound in the LBD (PDB 4NB6)[19] to select an additional 2000 compounds. The compounds were evaluated in a competitive binding assay using LBD of human RORγ. Compounds with >50% displacement were submitted for dose response to determine binding inhibitory constant (K_i) values. As expected, the overall hit rate was high (15% with K_i < 20 uM). Evaluation of active compounds followed by iterative selection and evaluation of structurally similar compounds from the Lilly collection identified several scaffolds of interest. These scaffolds were further narrowed based on SAR studies demonstrating the ability to adjust chemical properties such as calculated logarithm of partition coefficient between n-octanol and water (cLogP) while maintaining or improving potency. The 4′,5′-dihydrospiro[piperidine-4,7′-thieno[2,3-*c*]-

https://doi.org/10.1021/acs.jmedchem.0c01918
J. Med. Chem. 2021, 64, 5470−5484

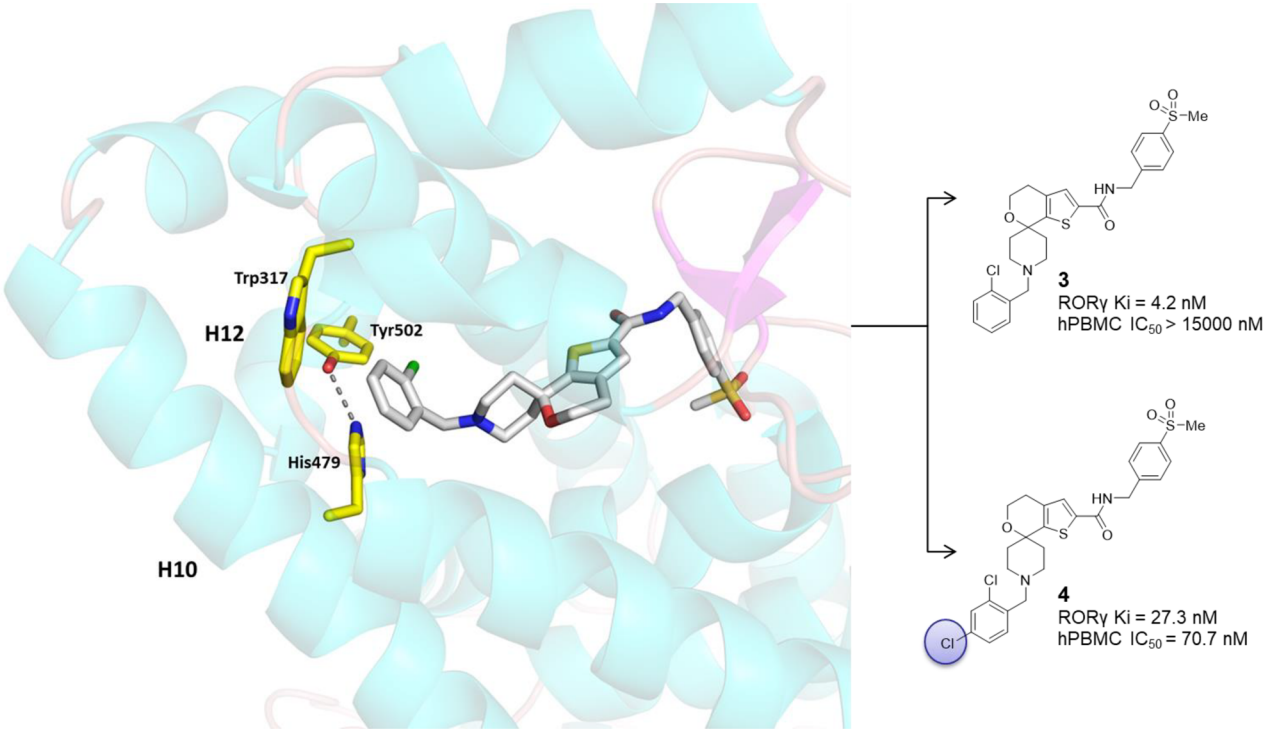

Figure 2. Co-crystal structure of compound **3** in the LBD of RORγ (PDB 7KCO).

pyran] scaffold represented by compounds **1** and **2** was selected for further evaluation based upon the potential to lower cLogP while maintaining or improving potency. Other active scaffolds generally had a cLogP > 4.5 and limited opportunity to improve potency without increasing lipophilicity.

Addition of the *N*-[4-(methylsulfonyl)benzyl] amide at C2 of the thiophene ring to give 1-benzyl-4′,5′-dihydrospiro-[piperidine-4,7′-thieno[2,3-*c*]pyran]-2′-carboxamides greatly improved the binding affinity and provided compound **3** as a starting point for further optimization. The utility of the benzylsulfone amide has been observed by other groups.[15] The structural basis for its contribution to binding affinity is described below. Compound **3** was evaluated for inhibition of IL- 17 secretion using human peripheral blood mononuclear cells (PBMCs). In general, inhibitor compounds were added to the PBMCs in a 10-point concentration response, and IL- 17 secretion was stimulated for 48 h by the addition of anti-CD3, anti-CD28, and IL-23. Supernatants were quantified for IL-17 content by ELISA. Unfortunately, although compound **3** exhibited excellent binding affinity, it failed to inhibit IL-17 secretion.

Structure-Based Design. After completing the virtual and binding screens and identifying compound **3**, we turned our attention to structural biology in order to design a scaffold with functional activity. A co-crystal structure of compound **3** with the LBD of RORγ was obtained (PDB 7KCO); see Figure 2. The increased affinity observed with addition of the benzylsulfone amide could now be attributed to hydrogen-bond interactions between the amide NH and Phe377 as well as sulfone interactions with Arg367 and the backbone NH of Leu287.

In general, the stability and position of helix 12, which forms the AF2 domain of nuclear receptors, is critical for co-regulator recruitment and subsequent functional activity.[20] The ROR family is unique in the class in that they have a conserved tyrosine (Tyr502) on helix 12 that forms a hydrogen bond to His479 on helix 10 (RORγ numbering).[16] The arrangement of hydrophobic amino acid side chains around an hydrogen bond in protein structures provides optimal stabilization.[21] We hypothesized that the Tyr502, His479 hydrogen bond is stabilized by Trp317 and that substitution of functional groups para to the benzylic carbon of compound **3** would project into this space and displace the indole of Trp317, potentially disrupting this critical hydrogen bond. In the event, adding a chlorine atom to compound **3** in the para position resulted in compound **4**, which inhibited IL-17 secretion from hPBMCs with a half-maximal inhibitory concentration (IC_{50}) of 70.7 nM. Similar dramatic shifts in activity have been described by other researchers, and a detailed molecular dynamics study of these observation has recently been reported.[22] Further optimization of the scaffold is described below.

Synthesis. The synthesis of the initial set of 1-benzyl-4′,5′-dihydrospiro[piperidine-4,7′-thieno[2,3-*c*]pyran]-2′-carboxamides is described in Scheme 1. Compound **5** was prepared as previously described.[23] Briefly, spiropiperidine **6** was synthesized from 2-(3-thienyl)ethanol and *t*-butylcarbonyl (Boc) protected piperidin-4-one in the presence of trifluoroacetic acid (TFA).[23] A carboxylate was selectively introduced at the C2 position of the thienopyranyl ring via metalation with *n*-BuLi and subsequent reaction with CO_2. 4-(Methylsulfonylphenyl)methanamine was coupled using HOBt and EDCI to provide compound **7**. The Boc protecting group was removed with 4 M HCl in dioxane to unmask the piperidine nitrogen, giving *N*-[4-(methylsulfonyl)benzyl]-4′,5′-dihydrospiro[piperidine-4,7′-thieno[2,3-*c*]pyran]-2′-carboxamide hydrochloride, which was reacted with benzyl bromides such as the 4-chlorobenzyl bromide depicted in Scheme 1 to provide final compounds analogous to compound **8** for testing. The compounds in Table 1 were prepared according to these

https://doi.org/10.1021/acs.jmedchem.0c01918
J. Med. Chem. 2021, 64, 5470−5484

Scheme 1. Synthesis of the Initial Set of 1-Benzyl-4′,5′-dihydrospiro[piperidine-4,7′-thieno[2,3-*c*]pyran]-2′-carboxamides[a]

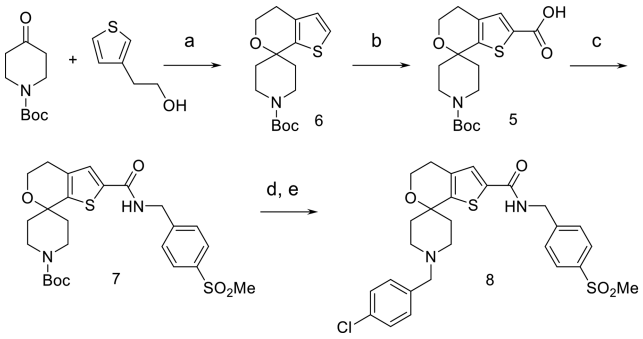

[a]Reagents and conditions: (a) TFA, CH_2Cl_2, RT; (b) *n*-BuLi, THF, CO_2, −78 °C; (c) 4-(methylsulfonylphenyl)methanamine, DIPEA, HOBt, EDCI, THF, DMF, RT; (d) 4 M HCl in dioxane, MeOH, RT; and (e) 4-chlorobenzyl bromide, ACN, DIPEA, RT.

procedures. In the case of compound **12**, 4-(ethylsulfonylphenyl)methanamine was coupled to the carboxylate **5**. The isomers of compounds **11** and **12** were separated using chiral HPLC.

A more advanced set of compounds with a 5′-methyl substitution on the spiropiperidine ring was prepared as depicted in Scheme 2. The C3 anion of thiophene was generated via lithium-halogen exchange of 3-bromothiophene with *sec*-butyllithium and then (2*S*)-2-methyloxirane was added followed by boron trifluoride diethyl etherate to afford (2*S*)-1-(3-thienyl)propan-2-ol **13**, which was then reacted with Boc-protected piperidin-4-one in the presence of TFA. Similar to as described above, the resulting compound **14** was Boc protected, and a carboxylate was then selectively introduced at the C2 position of the thienopyranyl ring. With compound **15** in hand, the next step was coupling to either (4-(ethylsulfonyl)phenyl)methanamine or 1-[5-(ethylsulfonyl)-pyridin-2-yl]methanamine to provide compounds **16**. After removing the Boc protecting group, the piperidine nitrogen could be alkylated with benzyl bromides to provide final compounds **17** for testing.

Medicinal Chemistry. The initial SAR studies focused on the benzyl group of compound **4** optimizing chemical properties while improving or maintaining receptor affinity and functional activity. In particular, this was a region where the cLogP could be lowered, which would likely result in better *in vivo* exposure; see Table 1. Analogous to compound **4**, moving the chlorine atom of **3** from the ortho position to the para position to provide compound **8** resulted in full inhibition but with a 9-fold loss of affinity. Replacing the Cl of **8** with a trifluoromethyl (**9**) had little impact on affinity or unbound human microsomal intrinsic clearance (hClint,u) as determined by microsomal stability.[24] This result was not surprising given that **4**, **8**, and **9** were relatively hydrophobic with a cLogP > 3.5. A para cyano group (**10**) however significantly lowered cLogP while maintaining receptor affinity and improved hClint,u. The addition of a methyl group to the benzyl carbon (**11**) improved affinity with only a small sacrifice in cLogP. Additionally, we found that replacing the methyl sulfone on the other side of the molecule with ethyl sulfone (**12**) improved both binding affinity and cellular potency. Despite the increase in cLogP, compound **12** maintained high sustained exposure in mice. All of these compounds demonstrated similar levels of cellular potency, inhibiting IL-17 secretion from hPBMCs with half-maximal inhibitory concentrations between 21 and 112 nM[25] and provided tools to assess PK/PD profiles in mice.

Mouse PK/PD and Efficacy. With these compounds in hand, we turned our attention toward defining the level of target engagement required for efficacy *in vivo*. Given that we would evaluate our compounds in mouse models, we obtained plasma exposure levels of compounds **9**, **11**, and **12** in mice with a 10 mg/kg dose. We used the IC_{50} values from the human PBMC assay as a surrogate for inhibition of IL-17 in a pharmacodynamic (PD) model in which mice were injected with an anti-CD3 antibody and recombinant human IL-23. The *in vitro* hPBMC assay was performed in the presence of 10% FBS, therefore potency values were corrected for the difference between *in vitro* and *in vivo* conditions using the method of Austin et al.[26] Briefly, the IC_{50} can be corrected using the unbound fraction (fu) in media 1 (plasma fu_1, C_1 = 100%) and media 2 (FBS fu_2, C_2 = 10%) and the following equation: corrected $IC_{50} \times fu_2/fu_1$, where $fu_2 = \frac{1}{\frac{C_2}{C_1}\left(\frac{1-fu_1}{fu_1}\right)+1}$.

As can be seen in Figure 3, plasma exposure levels of compounds **9** and **11** fell well below the corrected IC_{50} after 24 h; however, compound **12** provided plasma concentrations well above the corrected IC_{50} over a daily dosing interval. We used this exposure data along with physicochemical properties and Simcyp Simulator to estimate the steady-state oral pharmacokinetic (PK) profile of **12** in mice at 3, 10, 30, and 100 mg/kg doses to help design the PD study. The estimated PK curves and the corresponding measured PD responses are shown in Figure 4A,B, respectively. In order to more accurately define target engagement within the context of this model, we obtained an IC_{50} for inhibition of IL-17 secretion using stimulated mouse PBMCs in mouse plasma. We observed a 10-fold shift in potency from the corrected human PBMC IC_{50} of 180 nM to 1.8 μM. Significant inhibition was observed when exposure levels were maintained above the mouse plasma IC_{50} (black line = 1.8 μM) for about 20 to 24 h at the 30 and 100 mg/kg doses, respectively.

With this data in hand, we evaluated compound **12** for efficacy in the glucose-6-phosphate isomerase (GPI)-induced inflammatory arthritis mouse model.[27] The GPI-induced arthritis model is similar to the traditional rodent CIA model; however, the mice are immunized against GPI without the need for a boost. Acute inflammation is observed in the joints as early as day 4, and the animals can be successfully treated by blocking TNF, IL-6, or IL-17.[27,28] Mice were treated with compound **12** at the same doses used in the PD model (Figure 4D). A clinical score of efficacy was obtained as well as compound exposure levels in a subset of animals (Figure 4C). Maximal exposures were similar to predicted, and, although clearance was slightly higher, levels were maintained above the mouse plasma IC_{50} (black line = 1.8 μM) for approximately 20 h. This resulted in significant improvement of clinical score at the 10 and 30 mg/kg dose and nearly complete prophylaxis at the 100 mg/kg dose. We also measured IL-17 mRNA expression levels in the paws of a subset of animals (Figure 4E). Interestingly IL-17 expression was completely suppressed at the 3, 10, and 30 mg/kg doses, indicating that some of the inflammation observed in this model may not be RORγt dependent.

ADME, Human Dose, and PK Projections. Based on results from the mouse PD and GPI models, we determined

https://doi.org/10.1021/acs.jmedchem.0c01918
J. Med. Chem. 2021, 64, 5470−5484

Table 1. Evolution of 4′,5′-Dihydrospiro[piperidine-4,7′-thieno[2,3-*c*]pyran] RORγ Inhibitors

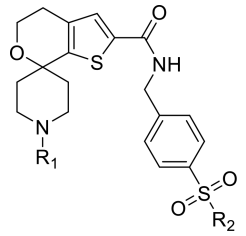

Compound	*R_1*	*R_2*	*hRORg Ki (nM)[a]*	*hPMBC IC_{50} (nM)[b]*	*cLogP / cLogD (7.4)[c]*	*hClint,u (mL/min/kg)[d]*
3	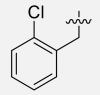	Me	4.2 (0.7)	>15000	3.9 / 3.4	4043
4	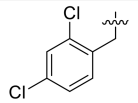	Me	27.3 (3.8)	70.7 (13)	4.5 / 4.3	3450
8	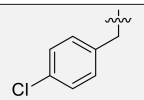	Me	249 (26)	64.0 (18)	3.9 / 3.4	495
9	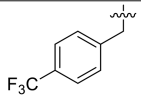	Me	249 (23)	112.0 (23)	4.1 / 3.4	448
10	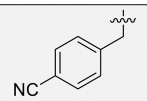	Me	278 (40)	95.1 (33)	3.1 / 2.5	80.7
11	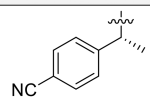	Me	94.6 (24)	50.1 (8.9)	3.5 / 2.8	218
12	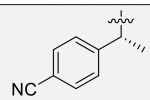	Et	15.8 (2.5)	21.7 (3.8)	4.0 / 3.6	406

[a]Binding assay: Competitive binding inhibitory constant (K_i) using radio-labeled [^{3}H]-25-hydroxycholesterol at the LBD of human RORγ ($n \geq 2$, SEM). [b]Functional assay: Inhibition of IL-17A secretion as measured by ELISA from aCD3/IL-23-stimulated human PBMCs ($n \geq 2$, SEM), [c]cLogP: Calculated octanol−water partition coefficient (LogP) using Chemaxon. cLogD: Calculated octanol−water distribution coefficient (LogD) at pH 7.4 using Chemaxon. [d]Unbound human microsomal intrinsic clearance based on percent remaining as determined by LC/MS in human microsomes after incubation for 30 min.

that maintaining plasma exposures above a cellular IC_{50} for at least 20 h would be the minimum requirement for a compound to advance to further evaluation. Although compound **12** was used successfully in mouse models to define advancement criteria, it was highly metabolized in human liver microsomes and its solubility in fasted state simulated intestinal fluid (FaSSIF) was very low at 0.0086 mg/mL. We hypothesized that these properties combined would limit absorption and exposure in larger animals required for safety studies and in the clinic. Indeed, we observed low and variable levels of exposure with this compound in dogs, and enabling formulations failed to improve absorption. The max absorbable dose and exposure in humans was predicted to be insufficient to allow exploration of desired exposure levels in the clinic that would maintain plasma concentrations above the IC_{50} observed in human PBMCs. Although the totality of these data represents a crude estimate of required target engagement and predicted clinical exposures, we determined that the risk of failure was too great and further improvements in physicochemical and ADME properties were necessary.

The compounds in Table 2 were designed with a focus on lowering cLogP and improving solubility and hClint,u, while maintaining binding affinity, cellular potency, and permeability. Compound **12** had excellent binding affinity and cellular potency with a reasonably low cLogP below 5; however, as noted above, it had poor solubility as well as high hClint,u. We discovered that a 2-(trifluoromethyl)pyrimidine group (**19**) was an excellent bioisostere for the benzonitrile of compound **12**. The corresponding (trifluoromethyl)benzene (**18**) is shown for comparison. All three compounds possessed nearly identical binding affinity and cellular potency. The 2-(trifluoromethyl)pyrimidine endowed compound **19** with a lower cLogP and correspondingly improved hClint,u. It also improved solubility, although by only 2-fold. By comparison, the (trifluoromethyl)benzene was more hydrophobic with a cLogP of 5.0. Many strategies were explored to further improve physicochemical properties, but they generally resulted in an

https://doi.org/10.1021/acs.jmedchem.0c01918
J. Med. Chem. 2021, 64, 5470−5484

Scheme 2. Synthesis of 5′-Methyl-Substituted 1-Benzyl-4′,5′-dihydrospiro[piperidine-4,7′-thieno[2,3-*c*]pyran]-2′-carboxamides[a]

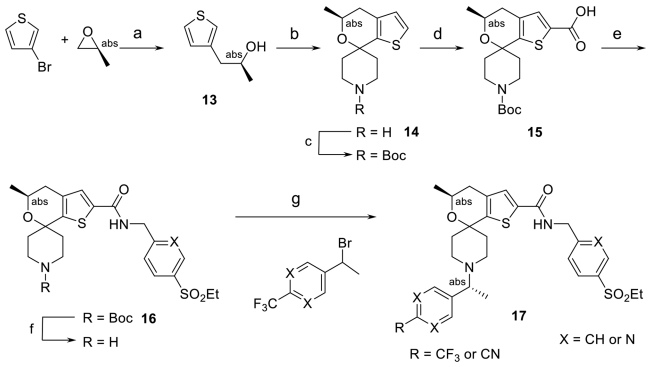

[a]Reagents and conditions: (a) sBuLi, $BF_3{\cdot}OEt_3$, THF, toluene −78 °C; (b) 1-Boc-piperidin-4-one, TFA, DCM, RT; (c) Boc_2O, DCM, RT; (d) *n*-BuLi, THF, CO_2, −78 °C; (e) (4-(ethylsulfonyl)phenyl)-methanamine or 1-[5-(ethylsulfonyl)pyridin-2-yl]methanamine, DIPEA, HOBt, EDCI, THF, RT; (f) 4 M HCl in dioxane, DCM, RT; and (g) appropriate benzyl bromide, ACN, K_2CO_3, 180 °C.

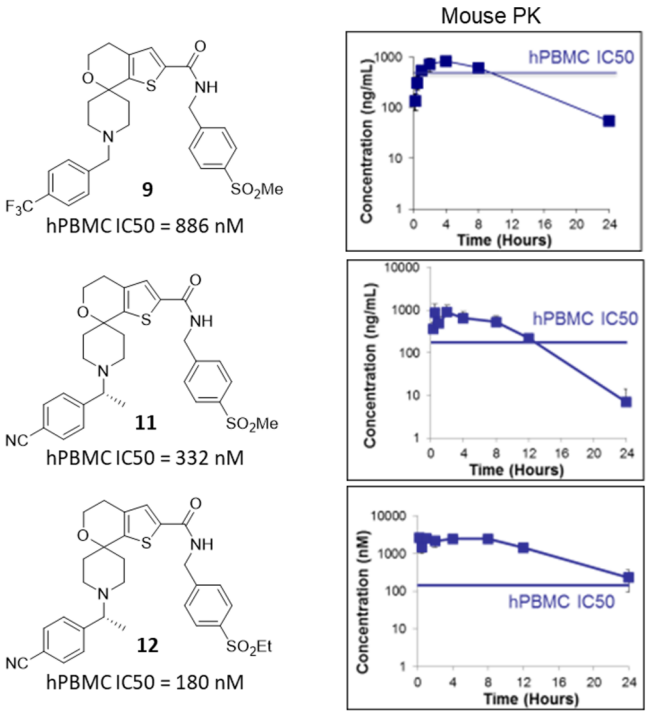

Figure 3. Exposure profiles and cellular IC_{50}. hPBMC IC_{50} corrected for protein binding differences *in vitro* vs *in vivo*.

unacceptable loss of binding affinity and cellular potency. Surprisingly, we found that the simple addition of a single methyl group at the 5′-carbon of the 4′,5′-dihydrospiro-[piperidine-4,7′-thieno[2,3-*c*]pyran] ring system to give compound **20** afforded an important 2- to 3-fold improvement in binding affinity, cellular potency, and solubility. We noted that this methyl group may fill a small hydrophobic pocket formed by Leu396, Lle397, Lle400, and Val480 that can be observed in the crystal structure of compound **3** with RORγ.

We also demonstrated that installing a nitrogen at the other end of the molecule, using a 1-[5-(ethylsulfonyl)pyridin-2-yl] group, instead of 4-(ethylsulfonylphenyl), afforded an impressive 22-fold improvement in solubility (compound **21** vs **12**). Finally, we also noted a significantly improved fraction unbound which provided reliable measurements to incorporate into the PBPK modeling described below. These observations motivated us to design and prepare compound **22**. We were delighted that the combination of these molecular changes was synergistic, affording a compound with similar binding affinity and cellular potency and with a cLogP < 3, excellent permeability, good solubility, and 12% fraction unbound in plasma, the totality of which would likely provide increased absorption and exposure with increasing doses. Compound **22** displayed no significant activity in kinase, nuclear receptor, GPCR, ion channel, or standard *in vitro* toxicology panel assays, including at hERG. In particular compound **22** had no measurable binding affinity to the closely related receptors RORα and RORβ (K_i > 15.5 μM and >20 μM, respectively.) Compound **22** was selected for further evaluation.

Compound **22** was selected as an RORγt inhibitor for use in patients with autoimmune diseases that respond well to anti-IL-17A antibodies, as has been demonstrated by the use of secukinumab[29] and ixekizumab[30] in psoriasis. Initial modeling efforts focused on identifying a target exposure of the small molecule that inhibits the secretion of IL-17A from human PBMCs stimulated with aCD3/aCD28/IL-23. The main risks associated with human dose projections in this context are the lack of animal models that translate to human disease and uncertainty with respect to how compound potency in the *in vitro* human PBMC assay can be linked to the potency of a drug's effect in patients. Therefore, the principal assumptions for the human dose projection strategy were as follows: (1) Human PK profiles can be predicted based on an understanding of gut absorption (permeability and solubility-driven), a mechanistic understanding of clearance, and *in vitro* and *in vivo* properties that support both clearance and volume of distribution predictions. (2) Memory T cells from pooled donor human PBMC stimulated with aCD3/IL-23 to produce IL-17A are mechanistically similar to the IL-17A producing cells that drive disease (i.e., IL-17A expression is RORγt dependent). (3) Target engagement for 24 h based on the *in vitro* PBMC assay is relevant and expected to lead to efficacy in patients. Based on target engagement data obtained in preclinical models as described above, we advanced compounds that were predicted to have human PK profiles sufficient to cover the corrected human PBMC IC_{50} and IC_{80} for 24 h.

For compound **22**, parameters that describe the human PK profile were derived from preclinical studies. The oral absorption parameters (F_a and k_a) were determined using solubility and permeability as well as absorption profiles from animal PK studies. Our initial human clearance prediction combined *in vitro* to *in vivo* scaling from hepatocytes with information on excretion pathways in preclinical species and human *in vitro* data. A PBPK model using Certara's Simcyp Simulator was applied to predict human PK.

Orally administered drugs tend to be metabolically cleared by hepatic first pass, thus the extrapolation of *in vitro* to *in vivo* clearance can be used to capture species differences in metabolism to then predict human clearance. *In vitro* and *in vivo* data indicated that the majority of compound **22** was cleared in rats and dogs by liver metabolism with only <2% through renal or biliary excretion. Therefore, a mathematical model[31] that describes liver metabolic clearance via blood flow, hepatic intrinsic clearance, and fraction unbound was used to

https://doi.org/10.1021/acs.jmedchem.0c01918
J. Med. Chem. 2021, 64, 5470−5484

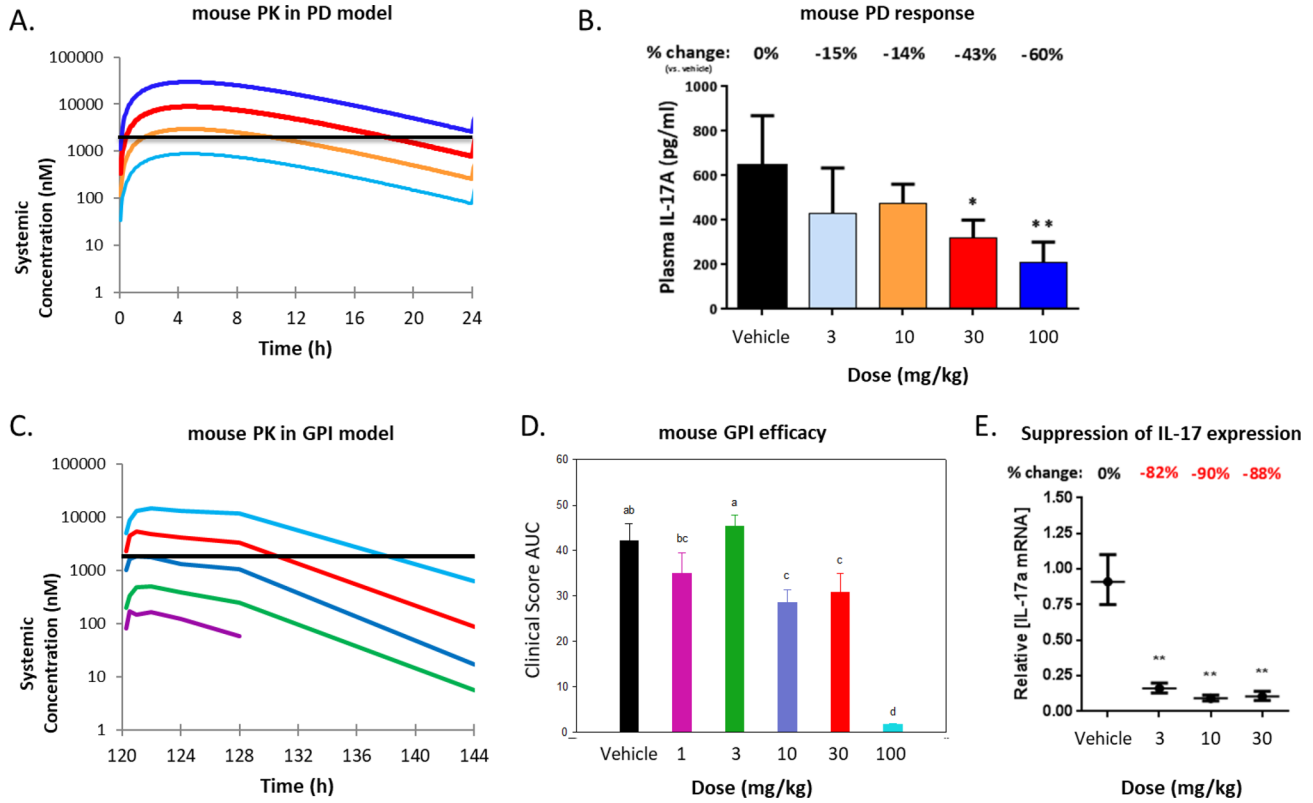

Figure 4. (A) Simulated systemic concentration in plasma over time of compound 12 in the mouse PD model. Black line is the IC_{50} for the inhibition of IL-17 secretion of stimulated mouse PBMCs in mouse plasma. (B) Response of compound **12** in mouse PD model. *P* values * <0.05 and **<0.01 using one-way ANOVA fit to the observed concentrations. (C) Measured systemic concentration in plasma over time of compound **12** in mouse GPI model. The time frame is 120−144 because the PK arm was taken on day 5 of the experiment. Black line is the IC_{50} for the inhibition of IL-17 secretion of stimulated mouse PBMCs in mouse plasma. (D) Efficacy of compound **12** in mouse GPI model. Different letters indicate significant difference (*p* value <0.05) using a one-way ANOVA followed by Turkey's post-test. (E) Suppression of IL-17 mRNA expression in paws from the mouse GPI model. *P* values **<0.01 using one-way ANOVA.

predict the fraction of compound **22** that remains in plasma after liver metabolism in animals and human (F_h). Compound **22** was primarily metabolized by CYP3A4 in human hepatocytes and is expected to undergo gut metabolism in humans during absorption; this intestinal effect was incorporated into the PBPK model to provide for the fraction that escapes gut metabolism (F_g). In addition, the volume of distribution was predicted using the Oie−Tozer method[32] and aligned with the output from Simcyp Simulator.

Predicted human PK parameters after simulation are presented in Table 3, and the predicted PK profiles are depicted in Figure 5. Clinical doses of compound **22** of 30 mg, BID or 80 mg, QD are predicted to achieve steady-state exposure (AUC_{0-24h} = 3507 or 4599 nM·h, respectively) that would achieve 50% inhibition of IL-17A production for 24 h. Both QD and BID dosing regimens are expected to achieve steady state after 3 days of dosing and provide concentrations above the corrected PBMC IC_{50} for 24 h. Higher predicted doses of 135 mg BID and 350 mg QD would be required to achieve coverage of the corrected PBMC IC_{80} concentrations for 24 h at steady state. The predicted human PK parameters and target engagement ratios (TER) are listed in Table 4.

DISCUSSION

Virtual screening and initial assessment of compounds active in a binding assay identified the 4′,5′-dihydrospiro[piperidine-4,7′-thieno[2,3-*c*]pyran] scaffold. An initial evaluation of this scaffold provided compound **3**, which served as a promising starting point for the design of potent RORγ inhibitors. Although compound **3** demonstrated very good affinity, it was functionally inactive. Analysis of an X-ray structure and structure-based design efficiently afforded a functionally active scaffold. Further optimization eventually provided compound **12**, which demonstrated very good activity in a mouse PK/PD model as well as efficacy in a mouse model of acute inflammation.

The design of a molecule suitable for clinical study required an understanding of the target engagement necessary for efficacy in humans. In order to build this knowledge base in a preclinical setting, we had to make a series of assumptions. We assumed that the memory T cells from pooled donor human PBMCs stimulated with aCD3/IL-23 to produce IL-17A are mechanistically similar to the IL-17A producing cells that drive disease (e.g., IL-17A expression is consistently RORγt dependent). We also assumed our human *in vitro* assay could be recapitulated in a rodent *in vivo* PD model (e.g., there would be a reasonable correlation between stimulated human PBMCs and a systemically stimulated mouse model). Finally, we assumed that the mouse PK/PD model would be reflective of PK/PD relationships in a clinical setting. Importantly, in order to correct for potential species differences, we elected to measure the IC_{50} for the inhibition of IL-17 secretion from stimulated mouse PBMCs in mouse plasma. We noted a

https://doi.org/10.1021/acs.jmedchem.0c01918
J. Med. Chem. 2021, 64, 5470−5484

Table 2. Optimization of Compound 12

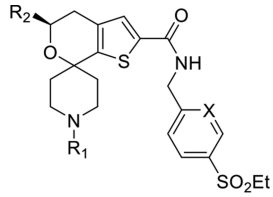

Cmpd	R_1	X	R_2	hRORg Ki (nM)[a]	hPMBC IC_{50} (nM)[b]	cLogP / cLogD (7.4)[c]	hClint,u (mL/min/kg)[d]	Papp (pH 7.4) MDCK[e]	FaSSIF (mg/mL)[f]	Fu[g]
12	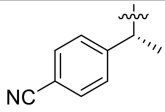	C	H	15.8 (2.5)	21.7 (3.8)	4.0 / 3.6	406	7.07	0.009	0.02
18	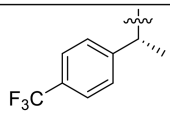	C	H	16.4 (4.0)	37.8 (11)	5.0 / 4.1	NA	NA	NA	NA
19	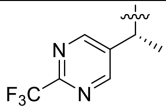	C	H	15.7 (9.1)	32.4 (6.1)	3.6 / 3.1	69.5	8.56	0.016	0.056
20	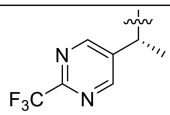	C	Me	5.89 (1.7)	10.6 (1.5)	4.0 / 3.5	36.2	7.57	0.024	0.041
21	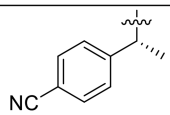	N	H	139 (68)	66.1 (14)	2.9 / 2.1	92.2	8.50	0.185	0.05
22	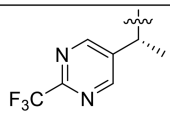	N	Me	16.6 (8.8)	22.0 (4.2)	2.9 / 2.4	32	9.07	0.22	0.12

[a]Binding assay: Competitive binding inhibitory constant (K_i) using radio-labeled [^{3}H]-25-hydroxycholesterol at the LBD of human RORγ ($n \geq 2$, SEM). [b]Functional assay: Inhibition of IL-17A secretion as measured by ELISA from aCD3/IL-23-stimulated human PBMCs ($n \geq 2$, SEM). [c]cLogP: Calculated octanol−water partition coefficient (LogP) using Chemaxon. cLogD: Calculated octanol−water distribution coefficient (LogD) at pH 7.4 using Chemaxon. [d]Unbound human microsomal intrinsic clearance based on percent remaining, as determined by LC/MS in human microsomes after incubation for 30 min. [e]Apparent permeability from apical-to-basolateral (A-to-B) at pH 7.4 using MDCK (Madin−Darby canine kidney) cells. [f]Solubility in FaSSIF. [g]Fraction unbound (fu) in human plasma.

Table 3. Predicted Human PK Parameters

parameter	value
F_a (1st order)	0.98
K_a (1/h)	0.77
CL (L/h)	21
CL_{po} (L/h)	39
F_g	0.81
F_h	0.74
F	0.58
V_{ss} (L/kg)	5.1
$T_{1/2}$(hr)	12
PBMC IC_{50} (nM)	89
PBMC IC_{80} (nM)	388

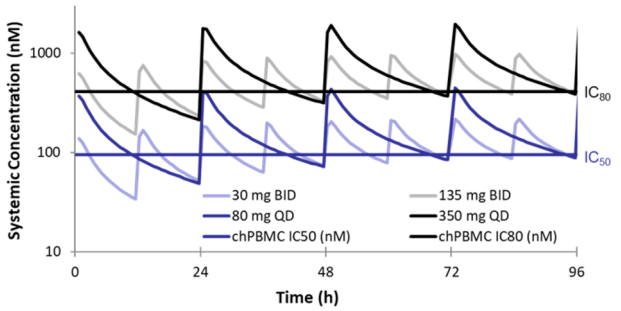

Figure 5. Compound **22** predicted human PK profiles at steady state.

significant shift in potency even with a correction for protein binding in the human PBMC assay.

With a good understanding of the PK/PD relationship in mice and data that served as a bridge to humans, we next needed to understand how the PD response observed in mice

https://doi.org/10.1021/acs.jmedchem.0c01918
J. Med. Chem. 2021, 64, 5470−5484

Table 4. Predicted Human PK and TER

Target Coverage over 24h	Dose	Predicted PK			Predicted TER	
	QD (mg)	C_{max} (nM)	Ctrough (nM)	AUC_{0-24} (nM*h)	C_{max}	Ctrough
IC_{50}	80	450	93	4599	4.8	1.0
IC_{80}	350	1967	407	20122	20.9	4.3
	BID (mg)					
IC_{50}	30	222	91	3507	2.4	1.0
IC_{80}	135	999	410	15783	10.6	4.4

related to efficacy. For this we used the GPI-induced arthritis model. Inherent in this strategy is the assumption that the acute inflammation observed in this model is reflective of the inflammation observed in human diseases known to be dependent on IL-17A. We were encouraged to make this assumption by the efficacy of anti-IL-17A antibodies in both the mouse model and the clinic. With these assumptions and the totality of the preclinical evidence obtained using compound **12**, we set as a minimum criteria for advancement to clinical trials, a molecule that could achieve plasma concentrations above the human PBMC IC_{50} for 24 h, similar to the coverage that provided efficacy observed in the mouse GPI model. Given the assumptions that were made and the limitations of preclinical models, we set as an additional criteria coverage of the human PBMC IC_{80} for 24 h.

CONCLUSIONS

Sufficient target engagement (TE) is necessarily the goal of target-based drug discovery efforts. Since a direct measurement of TE was not available to us, we demonstrated TE using a proximal and disease-relevant PD marker of RORγt activity, the expression of IL-17A and its secretion from IL-17A producing cells that was measured at each step in our discovery flow scheme from cell-based assays to animal models. Although compound **12** became a key molecule that was used to define TE requirements for efficacy in mouse models, its high metabolism in human liver microsomes and poor solubility made it unsuitable for clinical development. We therefore improved the physicochemical properties of the scaffold with guidance from simulations and modeling using the Simcyp Simulator. These efforts provided compound **22**, which was predicted to be capable of achieving in the clinic sufficient TE for the treatment of autoimmune diseases that are IL-17 dependent.

EXPERIMENTAL SECTION

Biology. All animal experiments were carried out according to an animal care and use protocol approved by the Eli Lilly Institutional Animal Care and Use Committees.

Binding assay. His-Flag-tagged human RORγ LBD (309−508) expressed in *E. coli* was used for receptor−ligand competition binding assays to determine K_i values. Receptor competition binding assays were run in a buffer of DPBS (1 L) (Hyclone #SH30028.03), 2.2 g of BSA fraction v (Roche #9048-46-8), 100 mL of glycerol (Fischer #56-81-5), and 40 mL of DMSO (reagent grade). The final wells contained 20 μg/mL of aprotinin and 20 μg/mL of leupeptin and 10 μM Pefabloc, radio-labeled [^{3}H]-25-hydroxycholesterol (6 nM), and 0.13 μg of RORγ receptor per well. Assays were run in 96-well format. Competing test compounds were added at various concentrations ranging from 0.4 nM to 25 μM. Nonspecific binding was determined in the presence of 250 nM 25-hydroxycholesterol. The sample, label, and receptor solutions were combined in a 96-well assay plate (Costar 3632) and incubated overnight at room temperature, then 25 μL of beads (Amersham YSi (2−5 μm) copper His-tag Spa Beads, #RPNQ0096) for a final bead concentration of 50 μg/well was added to each reaction. Plates were mixed for 30 min on an orbital shaker at room temperature. After an incubation of 4 h, plates were read in a Wallac MICROBETA counter. The data were used to calculate an estimated IC_{50} using a four parameter logistic fit. The K_d for [^{3}H]-25-hydroxycholesterol was determined by saturation binding. The IC_{50} values for compounds are converted to K_i using the Cheng−Prushoff equation.

Functional Assay. Stored human PBMCs isolated from whole blood buffy coats from 20 pooled donors were thawed and resuspended in RPMI 1640 (Hyclone, SH30255.02) supplemented with additional HEPES (5 mM) and L-glutamine (1.2 mM) plus fetal bovine serum (10%), pen/strep (100 U/mL), and β-mercaptoethanol (200 nM). After resuspension, 100,000 PBMCs per well were plated on 384-well tissue culture plates. Inhibitor compounds were added to the cells in a 10 pt. concentration response. IL- 17 secretion was stimulated for 48 h by the addition of antihuman-CD3 (Lilly, OKT3-RC), antihuman-CD28 (Lilly, IBA083), and human IL-23 (Lilly, 2821342), yielding 160 ng/mL, 500 ng/mL, and 5 ng/mL final concentrations in the assay. Supernatants were quantified for IL-17 content by ELISA (R&D Systems, MAB317/BAF317).

Mouse PBMC Assay. Whole blood was obtained from mice (129 strain) and collected via heparinized syringes into heparin tubes. An equal volume of whole blood (pooled from multiple different mice) was layered onto 1083 Histopaque separation media (Sigma #10831) in 15 mL tubes. To separate the red blood cells, the tubes were spun@ 400g for 30 min. Plasma was collected (without cells) and reserved for later use. The PBMC layer was collected and washed once with PBS. The PBMC cell pellet was then resuspended into the reserved plasma fraction. The cells were the counted and plated into deep-well 96-well plates in a volume of 150 μL, which contained between 200 and 400 K cells per well. The cells were pretreated with RORg inhibitor @ 25uM top dose, followed by 1:3 serial dilution in doses over a 10 point curve (1% DMSO final concentration). Cells were incubated with compound at 37 °C, 5% CO_2 for 2 h. Cells were stimulated with 40 ng aCD3 (Ebioscience #16-0031) and 80 ng IL23 (R&D systems #1290-IL-010) per well and incubated for 6 h at 37 °C, 5% CO_2. Cell pellets were then lysed for RNA extraction using the 5′ Perfect Pure Extraction Kit (#2900119). Subsequently, cDNA synthesis was performed using the Applied Biosystems High Capacity cDNA reverse transcription kit (#4322171). Taqman PCR was performed for mouse IL17A (Mm00439619_m1), mouse IL17F (Mm00521423_m1), and mouse actin (Mm00607939_s1), which was used as a normalizer. Data were calculated using the ddCT method.

Mouse PD Model. For all studies, female 129S6/SvEv mice (Taconic) of approximately 7−8 weeks of age were used, and studies were carried out under a protcol approved by the Eli Lilly Institutional Animal Care and Use Committee. Mice were group housed and maintained in a constant temperature and on a 12 h light/12 h dark cycle with free access to food and water at all times. Mice were randomly allocated to cages on arrival with adjustments made to ensure the average weight per cage was the same, with each cage being a separate study dose group (n = 5). Mice were dosed with either vehicle (1% hydroxyethylcellulose plus 0.25% Tween80 and 0.05% antifoam) or compound at 3, 10, 30, or 100 mg/kg and at a dose volume of 0.2 mL per mouse. Two h after dosing with compound, mice were challenged intraperitoneally with anti-CD3 (10 μg/mouse) and IL-23 (8 μg/mouse) in a 0.2 mL volume. Four h post-challenge, EDTA plasma was collected via cardiac puncture with blood spun

https://doi.org/10.1021/acs.jmedchem.0c01918
J. Med. Chem. 2021, 64, 5470−5484

down at 3000 rpm for 15 min to obtain plasma for measurement of circulating IL-17A. IL-17A was measured in the EDTA mouse plasma using an ELISA detection kit from R and D Systems. The ELISA methodology was as per the manufacturer's instructions. For statistical analysis, a robust one-way ANOVA model was fit to the observed concentrations. The single factor in the one-way model was the treatment group (compound and dose). Parameters of the model were fit to the data using robust regression as implemented by the rlm routine in the MASS package (version 7.3−35) in the R statistical software (version 3.1.2). Reported *p*-values were adjusted to account for multiple comparisons to the vehicle group using Dunnett's test implemented using the multcomp package (version 1.3−7) in the R statistical software.

Mouse GPI-Induced Arthritis Model. The mice were treated with GPI according to a previously published protocol[33] with a few modifications. Briefly, 4 mg/mL solution of recombinant human GPI was mixed with an equal volume of complete Freund's adjuvant. This final 2 mg/mL solution of GPI was used for the treatment. A 100 μL (200 μg) injection of the above solution was administered at both sides of the tail base to induce inflammation. Each paw was scored for severity of joint swelling based on a 0−3 scoring system (0 = normal, 1 = erythema and slight swelling of major joint, 2 = moderate to severe swelling of the major joint, and 3 = severe swelling of entire paw). The clinical score represents the total score of all 4 paws (maximum score = 12). Treatment with compound **12** started on the day of GPI immunization (day 0). The mice (n = 7−8/group) were treated once daily for 21 days. To capture the effect of treatment over time, clinical area under the curves (AUCs) were calculated. AUC was calculated by trapezoid method for clinical score over time from days 0 to 21. Clinical score AUC data are fitted with a one-way ANOVA model for treatment groups, and *p*-values were derived from model-based *t* test.

IL-17 mRNA Expression Levels in Mouse Paws. Paws were obtained from mice used in the GPI study and stored in liquid nitrogen. Whole paws were pulverized in a stainless steel cylinder/piston apparatus precooled with liquid nitrogen using a deadblow hammer. A portion of the pulverized mixture was used to isolate RNA in Lysing matrix D tubes (MPBio) containing ceramic beads and 1 mL of trizol. The mixture was further dissociated by two cycles of rapid agitation following by cooling on ice. RNA was then extracted by adding 1/10 volume BCP phase separation reagent (Sigma B9673), followed by mixing and centrifugation. A portion of the supernatant was collected and mixed with an equal volume of isopropanol. This mixture was purified over the 5 PRIME RNA purification 96-well kit, according to manufacturers instructions. Subsequently, cDNA synthesis was performed using the Applied Biosystems High Capacity cDNA reverse transcription kit (#4322171). Taqman PCR was performed for mouse IL17A (Mm00439619_m1), mouse IL17F (Mm00521423_m1), and mouse actin (Mm00607939_s1), which was used as a normalizer. Data were calculated using the ddCT method.

ADME. Animal protocols were approved and carried out under Covance Animal Care and Use Committee guidelines.

Microsomal Intrinsic Clearance. A fast gradient elution LC-MS/MS method was used to estimate the percent loss of substrate by Phase I metabolism in hepatic microsomes over a 30 min incubation period at 37 °C. Reactions were initiated with the addition of NADPH (0.5 mM) and terminated by protein precipitation with acetonitrile. The final substrate concentration was 2 μM in 100 mM sodium phosphate buffer, pH 7.4 with 0.5 mg/mL microsomal protein and a final organic solvent content of 0.5% acetonitrile and 0.02% DMSO. The ratio of the 30 min to the 0 min defined the percent remaining, and the value was converted to unbound intrinsic clearance using the rate of disappearance after correcting for microsomal protein binding. CLint,u is calculated using the following equation where fu, mic is assumed to be 1, or use calculated fu, or experimental fu if available:

$$\text{CLint, u} = [k \times (\text{liver wt/body wt}) \times (\text{protein/liver wt}) / \text{protein conc in incubation}]/\text{fu, mic}$$

Hepatocyte Intrinsic Clearance. Compounds (1 μM) were incubated at 37 °C with cryopreserved hepatocytes (1 million viable cells/mL) from rat, dog, or human were incubated at in a hepatocyte maintenance media for 90 min. At various time points, 20 μL samples were quenched with 80 μL of acetonitrile. Boiled hepatocytes were similarly incubated as controls. Compound disappearance was measured by LC/MS/MS, and intrinsic clearance was calculated using the rate of disappearance per million cells.

Fraction Unbound (Fu). A compound was added to human plasma or liver microsomes, mixed, and placed into a dialysis block with the plasma or microsomal mixture on one side and buffer on the other and incubated for 4.5 h. Samples were taken from both sides and analyzed by LC/MS/MS. Fraction unbound was calculated by dividing the concentration determined by LC/MS on the buffer side by that in the plasma or microsomal side.

MDCK Permeability. The test compound concentrations in this assay were 20 μM, and incubations were carried out at 37 °C with MDCK cells. Compound transport was measured in the absorptive direction and expressed as the percent transport (%T) over the incubation period. Benchmark compounds atenolol and dexamethasone were used to define levels of transport allowing test compounds to be classified as having low, medium, or high human intestinal absorption potential.

Fasted State Simulated Intestinal Fluid (FaSSIF) Solubility. Neat compound was weighed into sample vials. An appropriate volume of FaSSIF was added to the sample vial to achieve a target concentration of 2.0 mg/mL. Capped sample vials were placed in a rotation device to rotate through 360° for at least 16 h with an angular speed of approximately 50 rpm. Sample solution was filtered through a 0.7 μm glass fiber filter. The filtrate was analyzed by high-performance liquid chromatography (HPLC) assay for concentration against DMSO standard curve.

PK Studies. Compounds were orally dosed in a standard 1% hydroxyethylcellulose, 0.25% polysorbate 80, and 0.05% antifoam in purified water (HEC) formulation in all mouse studies, and serial microsamples of blood were collected and analyzed using the dried blood spot method.[34] Venous blood samples were serially collected at several time points after each dose in heparinized tubes, and plasma concentrations of test compounds were determined by LC/MS/MS. PK parameters were estimated based on a noncompartmental model analysis.

Chemistry. Reagents and solvents were used without additional purification. Compounds were characterized by HPLC using a gradient elution (10 mM NH_4HCO_3 in water; acetonitrile, 95:5−5:95) on a 2 × 50 Xbridge C18 3.5 um column with UV detection (200−400 nM). Flow rate = 1.2 mL/min, column temp = 50 °C. Purity of final compounds for assays was >95%. NMR chemical shifts are referenced to residual solvent.

*1-(tert-Butoxycarbonyl)-4′,5′-dihydrospiro[piperidine-4,7′-thieno[2,3-c]pyran]-2′-carboxylic acid (**5**).* *tert*-Butyl-4′,5′-dihydro-1H-spiro[piperidine-4,7′-thieno[2,3-c]pyran]-1-carboxylate **6** (10 g, 32.32 mmol) was dissolved in THF (100 mL) and cooled to −78 °C. To this was added butyllithium (22.22 mL, 35.55 mmol) dropwise over 15 min, and the mixture stirred an additional 15 min after addition was complete. CO_2 gas was added via cannula, and the mixture allowed to warm to room temperature with continuous addition of CO_2. After 2 h, the mixture was cooled to 0 °C, and water was added followed by Et_2O. The pH of the aqueous layer was adjusted with 1 N NaOH to basic pH. The organic layer was washed with 1 N NaOH (3×). The combined base washes were acidified to pH 2 with 5 N HCl. The aqueous layer was extracted with EtOAc (3×), and the organic extracts were combined, washed with brine, dried over sodium sulfate, filtered, and concentrated under reduced pressure to give a solid (11.11 g, 97%). ^{1}H NMR (399.80 MHz, d_6-DMSO): 7.43 (s, 1H), 3.87−3.82 (m, 2H), 3.14−3.13 (m, 2H), 2.62

https://doi.org/10.1021/acs.jmedchem.0c01918
J. Med. Chem. 2021, 64, 5470−5484

(t, J = 5.5 Hz, 2H), 2.48−2.46 (m, 2H), 1.95−1.92 (m, 2H), 1.67−1.60 (m, 2H), 1.38 (s, 9H). Mass spectrum (m/z): 352.2 (M-H).

*tert-Butyl 2′-{[4-(Methylsulfonyl)benzyl]carbamoyl}-4′,5′-dihydro-1H-spiro[piperidine-4,7′-thieno[2,3-c]pyran]-1-carboxylate (**7**).* DIPEA (14.8 mL, 84.9 mmol), HOBt (4.21, 31.1 mmol), and EDCI (5.97 g, 31.1 mmol) were added to **5** (10.0 g, 28.3 mmol) and 4-(methylsulfonylphenyl)methanamine hydrochloride (6.90 g, 31.1 mmol) in THF (100 mL) and DMF (100 mL) and stirred at ambient temperature for 16 h. The mixture was concentrated under reduced pressure until ∼1/2 volume, then water was added, and the mixture was extracted with DCM (3 × 100 mL). The combined DCM extracts were dried over sodium sulfate, filtered, and concentrated under reduced pressure. The material was purified by silica gel flash chromatography eluting with 50−100% EtOAc in hexanes to give a solid (14.0 g, 92%) as a white solid. ^{1}H NMR (399.80 MHz, d_6-DMSO): 9.09−9.06 (m, 1H), 7.86−7.83 (m, 2H), 7.52−7.50 (m, 3H), 4.49 (d, J = 6.0 Hz, 2H), 3.88−3.84 (m, 4H), 3.15 (s, 3H), 3.11−3.10 (m, 2H), 2.63−2.60 (m, 2H), 1.95−1.91 (m, 2H), 1.66−1.61 (m, 2H), 1.38 (s, 9H). Mass spectrum (m/z): 543 (M + Na), 465 (M-55), 421 (M-99).

N-[4-(Methylsulfonyl)benzyl]-4′,5′-dihydrospiro[piperidine-4,7′-thieno[2,3-c]pyran]-2′-carboxamide hydrochloride. HCl (4 M in 1,4-dioxane, 90 mL, 1.1 mol) was added to a solution of **7** (17.0 mg, 31.0 mmol) in 1,4-dioxane (90 mL) and methanol (30 mL) and then allowed to stir at ambient temperature for 4.0 h. The solution concentrated to ∼50% volume and filtered, and the precipitate was rinsed with DCM and dried under vacuum to give a solid (13.93 g, 98% yield). ^{1}H NMR (399.80 MHz, d_6-DMSO): 9.25−9.22 (m, 1H), 9.04−9.02 (m, 2H), 7.87−7.83 (m, 2H), 7.57 (s, 1H), 7.51 (d, J = 8.5 Hz, 2H), 4.49 (d, J = 6.0 Hz, 2H), 3.89−3.86 (m, 2H), 3.15 (s, 5H), 3.08−3.07 (m, 2H), 2.63 (t, J = 5.4 Hz, 2H), 2.10−2.06 (m, 4H). Mass spectrum (m/z): 421 (M + H).

*N-[4-(Methylsulfonyl)benzyl]-1-[4-(trifluoromethyl)benzyl]-4′,5′-dihydrospiro[piperidine-4,7′-thieno[2,3-c]pyran]-2′-carboxamide (**9**).* *N*-[4-(methylsulfonyl)benzyl]-4′,5′-dihydrospiro[piperidine-4,7′-thieno[2,3-*c*]pyran]-2′-carboxamide hydrochloride (0.95 g, 2.08 mmol) and 4-trifluoromethylbenzyl bromide (0.55 g, 2.29 mmol) were suspended in ACN (42 mL/g, 40 mL). DIPEA (0.80 mL, 4.57 mmol) was added, and the solution stirred at ambient temperature for 18 h. The solution was concentrated, diluted with EtOAc, and washed with aqueous saturated sodium bicarbonate and brine. The solution was dried with sodium sulfate, filtered, and concentrated under reduced pressure. The material was purified by silica gel flash chromatography eluting with a gradient of MeOH:DCM (0:100 to 5:95). Factions containing desired product were collected, concentrated, and lyophilized to give a solid (0.84 g, 70% yield). ^{1}H NMR (399.80 MHz, d_6-DMSO): 9.09−9.05 (m, 1H), 7.85 (d, J = 8.2 Hz, 2H), 7.66 (d, J = 8.3 Hz, 2H), 7.54−7.50 (m, 5H), 4.49 (d, J = 6.0 Hz, 2H), 3.83 (t, J = 5.4 Hz, 2H), 3.57 (s, 2H), 3.15 (s, 3H), 2.61−2.57 (m, 4H), 2.35−2.32 (m, 2H), 2.04−1.93 (m, 2H), 1.81−1.79 (m, 2H). Mass spectrum (m/z): 579 (M + H).

*1-(2-Chlorobenzyl)-N-[4-(methylsulfonyl)benzyl]-4′,5′-dihydrospiro[piperidine-4,7′-thieno[2,3-c]pyran]-2′-carboxamide (**3**).* ^{1}H NMR (399.80 MHz, d_6-DMSO): 9.09−9.05 (m, 1H), 7.86−7.84 (m, 2H), 7.52−7.50 (m, 4H), 7.41−7.38 (m, 1H), 7.33−7.30 (m, 2H), 4.49−4.47 (m, 2H), 3.86−3.83 (m, 2H), 3.57 (s, 2H), 3.15 (s, 3H), 2.63−2.61 (m, 4H), 2.44−2.42 (m, 2H), 1.96−1.93 (m, 2H), 1.81−1.79 (m, 2H). Mass spectrum (m/z): 545, 547 (M + H).

*1-(2,4-Dichlorobenzyl)-N-[4-(methylsulfonyl)benzyl]-4′,5′-dihydrospiro[piperidine-4,7′-thieno[2,3-c]pyran]-2′-carboxamide (**4**).* ^{1}H NMR (399.80 MHz, d_6-DMSO): 9.08−9.04 (m, 1H), 7.85−7.83 (m, 2H), 7.55−7.49 (m, 5H), 7.39 (dd, J = 2.1, 8.3 Hz, 1H), 4.49−4.47 (m, 2H), 3.84 (t, J = 5.4 Hz, 2H), 3.54 (s, 2H), 3.14 (s, 3H), 2.61−2.57 (m, 4H), 2.43−2.42 (m, 2H), 1.95−1.91 (m, 2H), 1.80−1.78 (m, 2H). Mass spectrum (m/z): 579.2, 581.2 (M + H)

*1-(4-Chlorobenzyl)-N-[4-(methylsulfonyl)benzyl]-4′,5′-dihydrospiro[piperidine-4,7′-thieno[2,3-c]pyran]-2′-carboxamide (**8**).* ^{1}H NMR (399.80 MHz, d_6-DMSO): 9.08−9.04 (m, 1H), 7.86−7.83 (m, 2H), 7.51−7.49 (m, 3H), 7.35−7.30 (m, 4H), 4.48 (d, J = 5.8 Hz, 2H), 3.84−3.81 (m, 2H), 3.53−3.46 (m, 2H), 3.14 (s, 3H), 2.60−2.54 (m, 4H), 2.32−2.29 (m, 2H), 1.93−1.89 (m, 2H), 1.79−1.75 (m, 2H). Mass spectrum (m/z): 545, 547 (M + H)

*1-(4-Cyanobenzyl)-N-[4-(methylsulfonyl)benzyl]-4′,5′-dihydrospiro[piperidine-4,7′-thieno[2,3-c]pyran]-2′-carboxamide (**10**).* ^{1}H NMR (399.80 MHz, d_6-DMSO): 9.08−9.05 (m, 1H), 7.86−7.83 (m, 2H), 7.77−7.74 (m, 2H), 7.52−7.49 (m, 5H), 4.48 (d, J = 5.8 Hz, 2H), 3.84−3.81 (m, 2H), 3.56 (s, 2H), 3.14 (s, 3H), 2.60−2.55 (m, 4H), 2.35−2.32 (m, 2H), 1.95−1.89 (m, 2H), 1.79−1.73 (m, 2H). Mass spectrum (m/z): 536 (M + H)

*(R)-1-(1-(4-cyanophenyl)ethyl)-N-(4-(methylsulfonyl)benzyl)-4′,5′-dihydrospiro[piperidine-4,7′-thieno[2,3-c]pyran]-2′-carboxamide (**11**).* Chiral purification of compound **11**. Isomers were separated using chiral HPLC [Chiralpak OJ-H, 35% MeOH (0.2% isopropylamine)/CO_2, flow rate = 5 mL/min, UV detection at 225 nm (monitored at 250 nm)]. Obtained **11**, isomer 1 (390 mg, ee >99%, R_t = 2.43 min) and isomer 2 (300 mg, ee >99%, R_t = 1.79 min). The desired isomer 1 was lyophilized to give a solid (390 mg, 32%). ^{1}H NMR (399.80 MHz, d_6-DMSO): 9.08−9.05 (m, 1H), 7.86−7.83 (m, 2H), 7.78−7.75 (m, 2H), 7.53−7.48 (m, 5H), 4.48 (d, J = 6.0 Hz, 2H), 3.80−3.77 (m, 2H), 3.60−3.57 (m, 1H), 3.15 (s, 3H), 2.76−2.74 (m, 1H), 2.58−2.55 (m, 2H), 2.45−2.47 (m, 1H), 2.31−2.29 (m, 2H), 1.99−1.96 (m, 2H), 1.81−1.79 (m, 2H), 1.27 (d, J = 6.8 Hz, 3H). Mass spectrum (m/z): 550 (M + H). Yielded undesired isomer was lyophilized to give a solid (300 mg, 25%). ^{1}H NMR (399.80 MHz, d_6-DMSO): 9.08−9.05 (m, 1H), 7.86−7.83 (m, 2H), 7.78−7.75 (m, 2H), 7.53−7.48 (m, 5H), 4.49−4.47 (m, 2H), 3.80−3.77 (m, 2H), 3.60−3.57 (m, 1H), 3.15 (s, 3H), 2.76−2.74 (m, 1H), 2.58−2.54 (m, 2H), 2.45−2.47 (m, 1H), 2.31−2.29 (m, 2H), 1.99−1.96 (m, 2H), 1.83−1.80 (m, 2H), 1.27 (d, J = 6.8 Hz, 3H). Mass spectrum (m/z): 550 (M + H).

*(R)-1-(1-(4-Cyanophenyl)ethyl)-N-(4-(ethylsulfonyl)benzyl)-4′,5′-dihydrospiro[piperidine-4,7′-thieno[2,3-c]pyran]-2′-carboxamide (**12**).* Chiral purification of compound **12**. Isomers were separated using chiral HPLC [Chiralpak AD-H 4.6 × 150 mm, 3/2 MeOH/0.2% isopropylamine in ACN, flow rate = 1 mL/min, UV detection at 225]. Obtained **12**, isomer 1 (77 mg, ee >99%, R_t = 2.65 min) and isomer 2 (78 mg, ee >99%, R_t = 4.63 min). The desired isomer 1 was lyophilized to give a solid (77 mg, 76%). ^{1}H NMR (399.80 MHz, d_6-DMSO): 9.08−9.05 (m, 1H), 7.82−7.76 (m, 4H), 7.53−7.48 (m, 5H), 4.51−4.48 (m, 2H), 3.81−3.78 (m, 2H), 3.61−3.60 (m, 1H), 3.22 (q, J = 7.4 Hz, 2H), 2.78−2.76 (m, 1H), 2.58−2.55 (m, 2H), 2.49−2.45 (m, 1H), 2.34−2.32 (m, 2H), 2.00−1.98 (m, 2H), 1.82−1.81 (m, 2H), 1.28−1.27 (m, 3H), 1.05 (t, J = 7.4 Hz, 3H). Mass spectrum (m/z): 564 (M + H). Yielded undesired isomer was lyophilized to give a solid (78 mg, 77%). ^{1}H NMR (399.80 MHz, d_6-DMSO): 9.08−9.05 (m, 1H), 7.82−7.75 (m, 4H), 7.53−7.49 (m, 5H), 4.50−4.47 (m, 2H), 3.81−3.78 (m, 2H), 3.61−3.60 (m, 1H), 3.25−3.20 (m, 2H), 2.76−2.74 (m, 1H), 2.58−2.55 (m, 2H), 2.49−2.45 (m, 1H), 2.31−2.30 (m, 2H), 1.99−1.98 (m, 2H), 1.81−1.80 (m, 2H), 1.28−1.26 (m, 3H), 1.05 (t, J = 7.3 Hz, 3H). Mass spectrum (m/z): 564 (M + H); see also Supporting Information.

*(2S)-1-(3-Thienyl)propan-2-ol (**13**).* 3-Bromothiophene (6.88 g, 42.2 mmol) was dissolved in anhydrous THF (10 mL) and toluene (100 mL). The solution was cooled to −78 °C. *sec*-Butyllithium (1.3 mol/L in cyclohexane, 34 mL, 44 mmol) was added over 15 min. The temperature was maintained at < −60 °C, stirred 10 min, and then (2*S*)-2-methyloxirane (4.9 g, 84.4 mmol) was added dropwise. After 5 min, boron trifluoride diethyl etherate (5.3 mL, 42 mmol) was added over 15 min. The temperature was maintained at < −55 °C. The mixture was stirred at −78 °C for 2 h. The reaction was quenched at −78 °C with saturated sodium bicarbonate. Et_2O was added, and the solution was warmed to ambient temperature. The solution was washed with saturated sodium bicarbonate (2×) and brine. The organic solution was dried over sodium sulfate, filtered, and concentrated under reduced pressure. The material was purified by silica gel flash chromatography eluting with 15% EtOAc/hexanes to give a colorless liquid (4.29 g, 71.5%). ^{1}H NMR (399.80 MHz, $CDCl_3$): 7.28 (dd, J = 3.0, 4.9 Hz, 1H), 7.03−7.02 (m, 1H), 6.96 (dd, J = 1.3, 4.9 Hz, 1H), 4.04−4.00 (m, 1H), 2.81 (dd, J = 4.7, 14.1 Hz,

https://doi.org/10.1021/acs.jmedchem.0c01918
J. Med. Chem. 2021, 64, 5470−5484

1H), 2.72 (dd, J = 7.9, 14.1 Hz, 1H), 1.60 (s, 2H), 1.23 (d, J = 6.2 Hz, 3H).

*(5′S)-5′-Methyl-4′,5′-dihydrospiro[piperidine-4,7′-thieno[2,3-c]-pyran] (**14**).* *tert*-Butyl 4-oxopiperidine-1-carboxylate (6.50 g, 32.6 mmol) and (2*S*)-1-(3-thienyl)propan-2-ol **13** (4.64g, 32.6 mmol) were dissolved in DCM (100 mL). Trifluoroacetic acid (20 mL, 264.5 mmol) was added. The mixture was stirred at ambient temperature for 18 h. The mixture was concentrated under reduced pressure, and then water and Et_2O were added. The organic solution was extracted with water. The pH of the combined aqueous extracts was adjusted with solid sodium carbonate. The aqueous layer was saturated with solid sodium chloride and extracted with EtOAc (5×). The combined EtOAc extracts were washed with brine, dried with sodium sulfate, filtered, and concentrated under reduced pressure to give a pale yellow oil (4.61g, 63%). ^{1}H NMR (399.80 MHz, d_6-DMSO): 7.30 (d, J = 5.1 Hz, 1H), 6.74 (d, J = 5.0 Hz, 1H), 3.88−3.85 (m, 1H), 3.25−3.23 (m, 1H), 2.89−2.80 (m, 4H), 2.59 (dd, J = 3.1, 15.8 Hz, 1H), 2.28 (dd, J = 10.5, 15.7 Hz, 1H), 2.03−1.99 (m, 1H), 1.78−1.70 (m, 1H), 1.59 (dq, J = 13.1, 2.6 Hz, 1H), 1.51−1.47 (m, 1H), 1.23 (d, J = 6.2 Hz, 3H). Mass spectrum (m/z): 224.2 (M + H).

tert-Butyl (5′S)-5′-Methyl-4′,5′-dihydro-1H-spiro[piperidine-4,7′-thieno[2,3-c]pyran]-1-carboxylate. **14** (10.39 g, 46.53 mmol) was dissolved in DCM (100 mL). Di-*tert*-butyl dicarbonate (11.52 mL, 51.18 mmol) was added dropwise, and the mixture stirred at ambient temperature for 1.5 h. Additional di-*tert*-butyl dicarbonate (2.00 mL, 9.17 mmol) was added. The solution was stirred for 30 min and then concentrated under reduced pressure. Imidazole (2.21 g, 32.5 mmol) was added to destroy excess di-*tert*-butyl dicarbonate. Et_2O was added, and the mixture was washed with brine. The organic solution was dried over sodium sulfate, filtered, and concentrated under reduced pressure. The material was purified by silica gel flash chromatography eluting with 10% EtOAc/hexanes. The material was further purified by silica gel flash chromatography eluting with 15% EtOAc/hexanes to give a colorless oil (12.92 g, 86%). ^{1}H NMR (400.13 MHz, d_6-DMSO) δ 7.33 (d, J = 5.1, 1H), 6.77 (d, J = 5.1, 1H), 3.92−3.72 (m, 3H), 3.15−2.91 (s, 2H), 2.62 (dd, J = 15.8, 3.0, 1H), 2.30 (dd, J = 15.8, 10.6, 1H), 2.1 (m, 1H), 1.76−1.63 (m, 2H), 1.51−1.40 (m, 1H), 1.38 (s, 9H), 1.24 (d, J = 6.2, 3H), 100% ee based on SFC chromatography, Lux Amylose-2, 5 mL/min, 225 nm, R_t = 1.75 min, OR $[\alpha]_D^{20}$ +82.1 (c 1.00, $CHCl_3$). Mass spectrum (m/z): 224.2 (M-99), 268 (M-55).

*(5′S)-1-tert-Butoxycarbonyl)-5′-methyl-4′,5′dihydrospiro-[piperidine-4,7′-thieno[2,3-c]pyran]-2′-carboxylic acid (**15**).* *tert*-Butyl (5′S)-5′-methyl-4′,5′-dihydro-1H-spiro[piperidine-4,7′-thieno-[2,3-*c*]pyran]-1-carboxylate (11.19 g, 34.60 mmol) was dissolved in anhydrous THF (200 mL) and cooled to −78 °C. *n*-Butyllithium (21 mL, 34.64 mmol) was added dropwise over 20 min. After addition was complete, the solution was stirred at −78 °C for 20 min, then CO_2 gas was added via cannula for 60 min. The mixture was warmed to room temperature with continuous addition of CO_2. After the solution was stirred 1 h at room temperature, the reaction was quenched with water (3 mL) and concentrated under reduced pressure to 25% volume. Et_2O and water were added. The mixture was extracted with water (2×), and the aqueous extracts were combined. The pH was adjusted to acidic pH with 1 N HCl. The aqueous layer was saturated with sodium chloride and extracted with EtOAc (2×). The combined EtOAc extracts were washed with brine, dried over sodium sulfate, filtered, and concentrated under reduced pressure to give a white foam (13.40 g, 100%). ^{1}H NMR (399.80 MHz, d_6-DMSO): 13.82−13.72 (m, 1H), 7.40 (s, 1H), 3.93−3.91 (m, 3H), 3.13−3.11 (m, 1H), 2.68−2.63 (m, 1H), 2.48−2.46 (m, 1H), 2.35−2.28 (m, 1H), 2.18−2.12 (m, 1H), 1.79−1.73 (m, 2H), 1.54−1.47 (m, 1H), 1.38 (s, 9H), 1.24 (d, J = 6.2 Hz, 3H). Mass spectrum (m/z): 366 (M − H).

*tert-Butyl (5′S)-2′-{[4-(Ethylsulfonyl)benzyl)carbamoyl}-5′-methyl-4′,5′-dihydro-1H-spiro[piperidine-4,7′-thieno[2,3-c]pyran]-1-carboxylate (**16**).* DIPEA (7.4 mL, 42 mmol), HOBt (1.80 g, 13 mmol), and EDCI (3.13 g, 16.3 mmol) were added to a slurry of **15** (4.44 g, 12.1 mmol) and 4-(ethylsulfonylphenyl)methanamine (3.42 g, 14.5 mmol) in DCM (100 mL) and stirred at ambient temperature for 16 h. Water was added, and the solution was extracted with DCM (3 × 100 mL). The combined DCM extracts were dried over sodium sulfate, filtered, and concentrated under reduced pressure. The material was purified using silica gel flash chromatography eluting with 50−100% EtOAc in hexanes to give a solid (4.24 g, 64%). ^{1}H NMR (399.83 MHz, $CDCl_3$): 7.85−7.84 (m, 2H), 7.54−7.51 (m, 2H), 7.25−7.22 (m, 3H), 6.57−6.56 (m, 1H), 4.72−4.70 (m, 2H), 4.04−4.03 (m, 3H), 3.29−3.28 (m, 1H), 3.15−3.13 (m, 3H), 2.65−2.64 (m, 1H), 2.50−2.49 (m, 1H), 2.16−2.15 (m, 1H), 1.91−1.90 (m, 1H), 1.70−1.69 (m, 1H), 1.59−1.55 (m, 1H), 1.47 (s, 9H), 1.38−1.36 (m, 3H), 1.28−1.23 (m, 3H). Mass spectrum (m/z): 449 (M-99), 493 (M-55), 549 (M + H), 571 (M + Na).

(5′S)-N-[4-(Ethylsulfonyl)benzyl]-5′-methyl-4′,5′-dihydrospiro-[piperidine-4,7′-thieno[2,3-c]pyran]-2′-carboxamide hydrochloride. HCl (4 mol/L in 1,4-dioxane, 15.6 mL, 62.4 mmol) was added to a solution of **16** (8.54 g, 15.57 mmol) in dry DCM (50 mL), and the mixture was stirred at ambient temperature for 1.5 h. The resulting solid was filtered and rinsed with DCM. The solid was dried under vacuum to give a solid (6.57 g, 87% crude). ^{1}H NMR (399.80 MHz, d_6-DMSO): 9.22−9.19 (m, 1H), 9.05−9.04 (m, 1H), 8.97−8.95 (m, 1H), 7.82−7.79 (m, 2H), 7.54−7.51 (m, 3H), 4.50−4.49 (m, 2H), 3.94−3.93 (m, 1H), 3.41−3.39 (m, 1H), 3.25−3.18 (m, 4H), 3.19−3.17 (m, 1H), 3.11−3.10 (m, 2H), 2.70−2.62 (m, 1H), 2.39−2.35 (m, 2H), 2.23−2.21 (m, 1H), 1.94−1.91 (m, 2H), 1.28−1.26 (m, 3H), 1.07−1.03 (m, 3H). Mass spectrum (m/z): 449 (M + H − HCl).

5-(1-Bromoethyl)-2-(trifluoromethyl)pyrimidine. 1-[2-(Trifluoromethyl)pyrimidin-5-yl]ethanol (1.663 g, 8.655 mmol) and triphenylphosphine (3.405 g, 12.98 mmol) were dissolved in DCM (86.55 mL), and NBS (12.98 mmol, 2.311 g) was added at room temperature. After 3 h, the solution was concentrated under reduced pressure. The material was purified using silica gel chromatography eluting with 10% EtOAc/hexanes to give a solid (1.641 g, 74.34%). ^{1}H NMR (400.13 MHz, d_6-DMSO) δ 9.26 (s, 2H), 5.63 (q, J = 7.0 Hz, 1H), 2.09 (d, J = 7.0 Hz, 3H). Mass spectrum (m/z): 255, 257 (M, M + 2).

*(5′S)-N-[4-(Ethylsulfonyl)benzyl]-5′-methyl-1-{(1R)-1-[2-(trifluoromethyl)pyrimidin-5-yl]ethyl}-4′,5′-dihydrospiro-[piperidine-4,7′-thieno[2,3-c]pyran]-2′-carboxamide (**20**).* (5′*S*)-*N*-[4-(Ethylsulfonyl)benzyl]-5′-methyl-4′,5′-dihydrospiro[piperidine-4,7′-thieno[2,3-*c*]pyran]-2′-carboxamide hydrochloride (10.73 g, 22.11 mmol) and 5-(1-bromoethyl)-2-(trifluoromethyl)pyrimidine (6.85 g, 26.85 mmol) were suspended in ACN (100 mL). Potassium carbonate (5.00 g, 36.17 mmol) was added. The reaction mixture was heated to reflux for 2 h. The mixture was cooled to ambient temperature, potassium carbonate (10.00 g, 72.34 mmol) was added, and the mixture was stirred for 18 h. Potassium carbonate (2.50 g, 18.08 mmol) was added, and the mixture heated to reflux for 1 h and then cooled to ambient temperature. The mixture was filtered, and the solids were rinsed with EtOAc. The filtrate was concentrated under reduced pressure. The mixture was diluted with EtOAc (100 mL) and washed with water (100 mL) and brine (100 mL). The solution was dried with sodium sulfate, filtered, and concentrated under reduced pressure to yield a solid (14.74 g). The enantiomers were separated with chiral chromatography using SFC [AD-H column (5 × 15 cm, with 27% IPA (20 mM NH_3) at 300 mL/min, injecting 8 mL (175 mg per injection) every 8 min, temperature = 35 °C, back pressure = 100 bar, UV detection at 280 nm]. Fractions containing the desired material were concentrated, dissolved in ACN (5 mL), and allowed to crystallize at room temperature. The excess solvent was removed under a stream of N_2 to give a solid (5.49 g, 40%). Chiral SFC (220 nm UV), column: AD-H 100 × 4.6 mm, 5 μm, mobile phase: 40% IPA/60% CO_2, isocratic: > 99% ee, > 99% de, R_t = 1.68 min. ^{1}H NMR (399.80 MHz, d_6-DMSO): 9.06−9.03 (m, 3H), 7.82−7.79 (m, 2H), 7.52−7.46 (m, 3H), 4.49 (d, J = 5.8 Hz, 2H), 3.89−3.86 (m, 2H), 3.22 (q, J = 7.4 Hz, 2H), 2.74−2.71 (m, 1H), 2.64−2.56 (m, 1H), 2.25−2.49 (m, 1H), 2.42−2.40 (m, 3H), 2.13−2.10 (m, 1H), 1.94−1.91 (m, 1H), 1.75−1.73 (m, 1H), 1.66−1.63 (m, 1H), 1.37 (d, J = 6.8 Hz, 3H), 1.18 (d, J = 6.1 Hz, 3H), 1.04 (t, J = 7.3 Hz, 3H). Mass spectrum (m/z): 623 (M + H).

https://doi.org/10.1021/acs.jmedchem.0c01918
J. Med. Chem. 2021, 64, 5470−5484

*N-[4-(Ethylsulfonyl)benzyl]-1-{(1R)-1-[4-(trifluoromethyl)phenyl]-ethyl}-4′,5′-dihydrospiro[piperidine-4,7′-thieno[2,3-c]pyran]-2′-carboxamide (**18**).* ^{1}H NMR (399.80 MHz, d_6-DMSO): 9.08−9.05 (m, 1H), 7.82−7.79 (m, 2H), 7.67−7.64 (m, 2H), 7.55−7.49 (m, 5H), 4.50−4.47 (m, 2H), 3.81−3.78 (m, 2H), 3.60−3.58 (m, 1H), 3.22 (q, J = 7.4 Hz, 2H), 2.79−2.78 (m, 1H), 2.58−2.56 (m, 2H), 2.33−2.32 (m, 2H), 2.00−1.99 (m, 2H), 1.83−1.81 (m, 2H), 1.29 (d, J = 6.7 Hz, 3H), 1.05 (t, J = 7.4 Hz, 3H). Mass spectrum (m/z): 607 (M + H).

*(5S′)-N-[4-(Ethylsulfonyl)benzyl]-1-{(1R)-1-[2-(trifluoromethyl)-pyrimidin-5-yl]ethyl}-4′,5′-dihydrospiro[piperidine-4,7′-thieno[2,3-c]pyran]-2′-carboxamide (**19**).* ^{1}H NMR (400.13 MHz, d_6-DMSO): 9.09−9.07 (m, 3H), 7.86−7.84 (m, 2H), 7.56−7.53 (m, 3H), 4.56−4.53 (m, 2H), 3.89−3.87 (m, 3H), 3.29−3.24 (m, 2H), 2.82−2.74 (m, 1H), 2.64−2.58 (m, 3H), 2.41−2.39 (m, 2H), 2.01−1.98 (m, 2H), 1.86−1.84 (m, 2H), 1.44−1.41 (m, 3H), 1.09 (t, J = 7.3 Hz, 3H). Mass spectrum (m/z): 609 (M + H).

*1-[(1R)-1-(4-Cyanophenyl)ethyl]-N-{[5-(ethylsulfonyl)pyridin-2-yl]methyl}-4′,5′-dihydrospiro[piperidine-4,7′-thieno[2,3-c]pyran]-2′-carboxamide (**21**).* ^{1}H NMR (400.13 MHz, d_6-DMSO): 9.18 (t, J = 5.9 Hz, 1H), 8.96 (d, J = 2.0 Hz, 1H), 8.25 (dd, J = 2.2, 8.2 Hz, 1H), 7.80 (d, J = 8.1 Hz, 2H), 7.58−7.56 (m, 4H), 4.63 (d, J = 5.8 Hz, 2H), 3.84 (t, J = 5.4 Hz, 2H), 3.64−3.60 (m, 1H), 3.39 (q, J = 7.3 Hz, 2H), 2.81−2.73 (m, 1H), 2.62 (t, J = 5.2 Hz, 2H), 2.55−2.48 (m, 1H), 2.35−2.26 (m, 2H), 2.01−1.93 (m, 2H), 1.85−1.77 (m, 2H), 1.32 (d, J = 6.7 Hz, 3H), 1.13 (t, J = 7.3 Hz, 3H). Mass spectrum (m/z): 565 (M + H).

*(5S′)-N-{[5-(Ethylsulfonyl)pyridine-2-yl]methyl}-5′-methyl-1-{(1R)-1-[2-(trifluoromethyl)pyrimidin-5-yl]ethyl}-4′,5′-dihydrospiro-[piperidine-4,7′-thieno[2,3-C]pyran]-2′-carboxamide (**22**).* ^{1}H NMR (400.13 MHz, $CDCl_3$): 9.05 (d, J = 2.0 Hz, 1H), 8.91 (s, 2H), 8.16 (dd, J = 2.1, 8.2 Hz, 1H), 7.54 (d, J = 8.2 Hz, 1H), 7.26 (d, J = 2.5 Hz, 2H), 7.11 (t, J = 5.1 Hz, 1H), 4.82 (d, J = 5.3 Hz, 2H), 3.91−3.85 (m, 1H), 3.69 (q, J = 6.5 Hz, 1H), 3.16 (q, J = 7.4 Hz, 2H), 2.83−2.77 (m, 1H), 2.64−2.45 (m, 5H), 2.14−2.03 (m, 2H), 1.92 (dd, J = 2.5, 13.5 Hz, 1H), 1.85−1.76 (m, 1H), 1.46 (d, J = 6.6 Hz, 3H), 1.34−1.30 (m, 6H). Mass spectrum (m/z): 624 (M + H).

■ ASSOCIATED CONTENT

Supporting Information

The Supporting Information is available free of charge at https://pubs.acs.org/doi/10.1021/acs.jmedchem.0c01918.

HPLC traces for compounds **12** and **22**. X-ray data and refinement statistics (PDF)

Molecular formula strings; crystallographic information (CSV)

Accession Codes

Authors have released atomic coordinates and experimental data (PDB code 7KCO for compound **3** bound to the LBD of RORγ).

■ AUTHOR INFORMATION

Corresponding Author

Charles W. Lugar − *Lilly Research Laboratories, Eli Lilly and Company, Indianapolis, Indiana 46285, United States;* orcid.org/0000-0001-6313-5859; Phone: 317-277-0325; Email: lugar_charles_w@lilly.com

Authors

Christian A. Clarke − *Lilly Research Laboratories, Eli Lilly and Company, Indianapolis, Indiana 46285, United States*

Richard Morphy − *Lilly Research Laboratories, Eli Lilly and Company, Indianapolis, Indiana 46285, United States*

Helene Rudyk − *Lilly Research Laboratories, Eli Lilly and Company, Indianapolis, Indiana 46285, United States*

Selma Sapmaz − *Lilly Research Laboratories, Eli Lilly and Company, Indianapolis, Indiana 46285, United States*

Ryan E. Stites − *Lilly Research Laboratories, Eli Lilly and Company, Indianapolis, Indiana 46285, United States*

Grant M. Vaught − *Lilly Research Laboratories, Eli Lilly and Company, Indianapolis, Indiana 46285, United States*

Kelly Furness − *Lilly Research Laboratories, Eli Lilly and Company, Indianapolis, Indiana 46285, United States*

Howard B. Broughton − *Lilly Research Laboratories, Eli Lilly and Company, Indianapolis, Indiana 46285, United States*

Greg L. Durst − *Lilly Research Laboratories, Eli Lilly and Company, Indianapolis, Indiana 46285, United States*

David K. Clawson − *Lilly Research Laboratories, Eli Lilly and Company, Indianapolis, Indiana 46285, United States*

Stephanie L. Stout − *Lilly Research Laboratories, Eli Lilly and Company, Indianapolis, Indiana 46285, United States*

Sherry Y. Guo − *Lilly Research Laboratories, Eli Lilly and Company, Indianapolis, Indiana 46285, United States*

Jim D. Durbin − *Lilly Research Laboratories, Eli Lilly and Company, Indianapolis, Indiana 46285, United States*

Keith R. Stayrook − *Lilly Research Laboratories, Eli Lilly and Company, Indianapolis, Indiana 46285, United States*

Denise D. Edmondson − *Lilly Research Laboratories, Eli Lilly and Company, Indianapolis, Indiana 46285, United States*

Kristy Kikly − *Lilly Research Laboratories, Eli Lilly and Company, Indianapolis, Indiana 46285, United States*

Nicole E. New − *Lilly Research Laboratories, Eli Lilly and Company, Indianapolis, Indiana 46285, United States*

Holly A. Bina − *Lilly Research Laboratories, Eli Lilly and Company, Indianapolis, Indiana 46285, United States*

Mark G. Chambers − *Lilly Research Laboratories, Eli Lilly and Company, Indianapolis, Indiana 46285, United States*

Pamela Shetler − *Lilly Research Laboratories, Eli Lilly and Company, Indianapolis, Indiana 46285, United States*

William Y. Chang − *Lilly Biotechnology Center, Eli Lilly and Company, San Diego, California 92121, United States*

Veavi Ching-Yun Chang − *Lilly Research Laboratories, Eli Lilly and Company, Indianapolis, Indiana 46285, United States*

Rob Barr − *Lilly Research Laboratories, Eli Lilly and Company, Indianapolis, Indiana 46285, United States*

Wendy H. Gough − *Lilly Research Laboratories, Eli Lilly and Company, Indianapolis, Indiana 46285, United States*

Jimmy P. Steele − *Lilly Research Laboratories, Eli Lilly and Company, Indianapolis, Indiana 46285, United States*

Brian Getman − *Lilly Research Laboratories, Eli Lilly and Company, Indianapolis, Indiana 46285, United States*

Nita Patel − *Lilly Research Laboratories, Eli Lilly and Company, Indianapolis, Indiana 46285, United States*

Brian M. Mathes − *Lilly Research Laboratories, Eli Lilly and Company, Indianapolis, Indiana 46285, United States*

Timothy I. Richardson − *Lilly Research Laboratories, Eli Lilly and Company, Indianapolis, Indiana 46285, United States*

Complete contact information is available at: https://pubs.acs.org/10.1021/acs.jmedchem.0c01918

Author Contributions

C.W.L.: Designed and prepared compounds, summarized and interpreted results, and contributed to and reviewed the manuscript. C.A.C., J.R.M., H.R., S.S., R.E.S., G.M.V., and K.F.: Designed and prepared compounds and interpreted results; H.B.B. and G.L.D.: Designed, conducted, and interpreted the virtual screen, D.K.C., S.L.S., and S.Y.G.: Conducted and

summarized structural biology studies. J.D.D.: Interpreted structural biology results and contributed to the manuscript. K.R.S.: Designed biological studies, reviewed, interpreted and summarized results, and contributed to and reviewed the manuscript. D.D.E.: Designed, conducted, interpreted, and summarized *in vitro* studies. K.K.: Designed and interpreted biological studies. N.E.N. and H.A.B.: Conducted and summarized biological studies. M.G.C.: Interpreted and summarized results from *in vivo* PD studies and reviewed the manuscript. P.S.: Conducted *in vivo* PD studies. W.Y.C.: Designed the GPI mouse model, interpreted and summarized results from *in vivo* studies, and reviewed the manuscript. C.V.: Statistical analyses and reviewed and interpreted data; R.B., W.H.G., J.P.S., and B.G.: Designed, conducted. and interpreted *in vitro* assays. N.P.: Designed, interpreted, and summarized ADME and PK studies, performed human PK predictions, and contributed to and reviewed the manuscript. B.M.M.: Designed and prepared formulations. T.I.R.: Designed compounds and studies, reviewed, interpreted and summarized results, and wrote the manuscript.

Notes

The authors declare the following competing financial interest(s): All authors are current or former employees of Eli Lilly and Company.

■ ABBREVIATIONS USED

ACN, acetonitrile; AF1, activation function 1; AF2, activation function 2; ANOVA, analysis of variance; BID, twice a day; Boc, *t*-butoxycarbonyl; CL, clearance; cLogP, calculated octanol−water partition coefficient; CYP, cytochrome P450 enzyme; DCM, dichloromethane; DIPEA, di-isopropylethylamine; EDCI, 1-ethyl-3-(3-(dimethylamino)propyl)-carbodiimide; EtOAc, ethyl acetate; *F*, fraction absorbed (bioavailability); FaSSIF, fasted state simulated intestinal fluid; F_h, fraction after liver metabolism; F_g, fraction after gut metabolism; GPI, glucose-6-phosphate isomerase; hClint, u, unbound human microsomal intrinsic clearance; HOBt, hydroxybenzotriazole; HPLC, high-performance liquid chromatography; IPA, isopropyl alcohol; LBD, ligand binding domain; IL, interleukin; LTi, lymphoid tissue inducer; K_a, first-order absorption rate; NBS, *N*-bromosuccinamide; NK, natural killer; PBMC, peripheral blood mononuclear cells; PBPK, physiologically-based pharmacokinetic; PK, pharmacokinetics; QD, once a day; RT, room temperature; SAR, structure−activity relationship; $T_{1/2}$, half-life; Th, t-helper; THF, tetrahydrofuran; TE, target engagement; TER, target engagement ratio; TFA, trifluoroacetic acid; V_{ss}, steady-state volume of distributibution

■ REFERENCES

(1) Cooper, G. S.; Bynum, M. L.K.; Somers, E. C. Recent insights in the epidemiology of autoimmune diseases: improved prevalence estimates and understanding of clustering of diseases. *J. Autoimmun.* **2009**, *33* (3−4), 197−207.

(2) Gaffen, S. L.; Jain, R.; Garg, A. V.; Cua, D. J. The IL-23-IL-17 immune axis: from mechanisms to therapeutic testing. *Nat. Rev. Immunol.* **2014**, *14*, 585−600.

(3) Kanai, T.; Mikami, Y.; Sujino, T.; Hisamatsu, T.; Hibi, T. RORγt-dependent IL-17a-producing cells in the pathogenesis of intestinal inflammation. *Mucosal Immunol.* **2012**, *5* (3), 240−247.

(4) Robinson-Rechavi, M.; Garcia, H. E.; Laudet, V. The nuclear receptor superfamily. *J. Cell Sci.* **2003**, *116*, 585−586.

(5) (a) Jin, L.; Martynowski, D.; Zheng, S.; Wada, T.; Xie, W.; Li, Y. Structural basis for hydroxycholesterols as natural ligands of orphan nuclear receptor RORγ. *Mol. Endocrinol.* **2010**, *24* (5), 923−929. (b) Soroosh, P.; Wu, J.; Xue, X.; Song, J.; Sutton, S. W.; Sablad, M.; Yu, J.; Nelen, M. I.; Liu, X.; Castro, G.; Luna, R.; Crawford, S.; Banie, H.; Dandridge, R. A.; Deng, X.; Bittner, A.; Kuei, C.; Tootoonchi, M.; Rozenkrants, N.; Herman, K.; Gao, J.; Yang, X. V.; Sachen, K.; Ngo, K.; Fung-Leung, W. P.; Nguyen, S.; de Leon-Tabaldo, A.; Blevitt, J.; Zhang, Y.; Cummings, M. D.; Rao, T.; Mani, N. S.; Liu, C.; McKinnon, M.; Milla, M. E.; Fourie, A. M.; Sun, S. Oxysterols are agonist ligands of RORγt and drive Th17 cell differentiation. *Proc. Natl. Acad. Sci. U. S. A.* **2014**, *111* (33), 12163−12168.

(6) (a) Santori, F. R.; Huang, P.; van de Pavert, S. A.; Douglass, E. F., Jr.; Leaver, D. J.; Haubrich, B. A.; Keber, R.; Lorbek, G.; Konijn, T.; Rosales, B. N.; Rozman, D.; Horvat, S.; Rahier, A.; Mebius, R. E.; Rastinejad, F.; Nes, W. D.; Littman, D. R. Identification of natural RORγ ligands that regulate the development of lymphoid cells. *Cell Metab.* **2015**, *21*, 286−298. (b) Hu, X.; Wang, Y.; Hao, L.-Y.; Liu, X.; Lesch, C. A.; Sanchez, B. M.; Wendling, J. M.; Morgan, R. W.; Aicher, T. D.; Carter, L. L.; Toogood, P. L.; Glick, G. D. Sterol metabolism controls TH17 differentiation by generating endogenous RORγ agonists. *Nat. Chem. Biol.* **2015**, *11*, 141−147.

(7) We have chosen to use target name RORγt in the context of immunology; however, in the context of medicinal chemistry, we will use RORγ since the compounds do not discriminate between the two isoforms.

(8) Ran, D.; Cai, M.; Zhang, X. Genetics of psoriasis: a basis for precision medicine. *Precis Clin Medicine* **2019**, *2* (2), 120−130.

(9) Bowes, J.; Budu-Aggrey, A.; Huffmeier, U.; Uebe, S.; Steel, K.; Hebert, H. L.; Wallace, C.; Massey, J.; Bruce, I. N.; Bluett, J.; Feletar, M.; Morgan, A. W.; Marzo-Ortega, H.; Donohoe, G.; Morris, D. W.; Helliwell, P.; Ryan, A. W.; Kane, D.; Warren, R. B.; Korendowych, E.; Alenius, G.-M.; Giardina, E.; Packham, J.; McManus, R.; FitzGerald, O.; McHugh, N.; Brown, M. A.; Ho, P.; Behrens, F.; Burkhardt, H.; Reis, A.; Barton, A. Dense Genotyping of immune-related susceptibility loci reveals new insights into the genetics of psoriatic arthritis. *Nat. Commun.* **2015**, *6* (1), 6046.

(10) Tsui, F. W.; Tsui, H. W.; Akram, A.; Haroon, N.; Inman, R. D. The genetic basis of ankylosing spondylitis: new insights into disease pathogenesis. *Appl. Clin. Genet.* **2014**, *7*, 105−115.

(11) Okada, S.; Markle, J. G.; Deenick, E. K.; Mele, F.; Averbuch, D.; Lagos, M.; Alzahrani, M.; Al-Muhsen, S.; Halwani, R.; Ma, C. S.; Wong, N.; Soudais, C.; Henderson, L. A.; Marzouqa, H.; Shamma, J.; Gonzalez, M.; Martinez-Barricarte, R.; Okada, C.; Avery, D. T.; Latorre, D.; Deswarte, C.; Jabot-Hanin, F.; Torrado, E.; Fountain, J.; Belkadi, A.; Itan, Y.; Boisson, B.; Migaud, M.; Arlehamn, C. S. L.; Sette, A.; Breton, S.; McCluskey, J.; Rossjohn, J.; de, Villartay J. P.; Moshous, D.; Hambleton, S.; Latour, S.; Arkwright, P. D.; Picard, C.; Lantz, O.; Engelhard, D.; Kobayashi, M.; Abel, L.; Cooper, A. M.; Notarangelo, L. D.; Boisson-Dupuis, S.; Puel, A.; Sallusto, F.; Bustamante, J.; Tangye, S. G.; Casanova, J. Impairment of immunity to candida and mycobacterium in humans with bi-allelic RORC mutations. *Science* **2015**, *349* (6248), 606−613.

(12) Fauber, B. P.; Magnuson, S. Modulators of the nuclear receptor retinoic acid receptor-related orphan receptor-γ (RORγ or RORc). *J. Med. Chem.* **2014**, *57* (14), 5871−5892.

(13) (a) Ueda, E.; Kurebayashi, S.; Sakaue, M.; Backlund, M.; Koller, B.; Jetten, A. M. High incidence of t-cell lymphomas in mice deficient in the retinoid-related orphan receptor RORγ. *Cancer Res.* **2002**, *62* (3), 901−909. (b) Liljevald, M.; Rehnberg, M.; Söderberg, M.; Ramnegård, M.; Börjesson, J.; Luciani, D.; Krutrök, N.; Brändén, L.; Johansson, C.; Xu, X.; Bjursell, M.; Sjögren, A. K.; Hornberg, J.; Andersson, U.; Keeling, D.; Jirholt, J. Retinoid-related orphan receptor γ (RORγ) adult induced knockout mice develop lymphoblastic lymphoma. *Autoimmun. Rev.* **2016**, *15* (11), 1062−1070.

(14) Guntermann, C.; Piaia, A.; Hamel, M.-L.; Theil, D.; Rubic-Schneider, T.; del Rio-Espinola, A.; Dong, L.; Billich, A.; Kaupmann, K.; Dawson, J.; Hoegenauer, K.; Orain, D.; Hintermann, S.; Stringer, R.; Patel, D. D.; Doelemeyer, A.; Deurinck, M.; Schümann, J.

https://doi.org/10.1021/acs.jmedchem.0c01918
J. Med. Chem. 2021, 64, 5470−5484

Retinoic-acid-orphan-receptor-c inhibition suppresses Th17 cells and induces thymic aberrations. *JCI Insight* **2017**, *2* (5), 1−16.
(15) Jetten, A. M.; Cook, D. N. (Inverse) Agonists of retinoic acid-related orphan receptor γ: regulation of immune responses, inflammation, and autoimmune disease. *Annu. Rev. Pharmacol. Toxicol.* **2020**, *60* (1), 371−390.
(16) Li, X.; Anderson, M.; Collin, D.; Muegge, I.; Wan, J.; Brennan, D.; Kugler, S.; Terenzio, D.; Kennedy, C.; Lin, S.; Labadia, M. E.; Cook, B.; Hughes, R.; Farrow, N. A. Structural studies unravel the active conformation of apo RORγt nuclear receptor and a common inverse agonism of two diverse classes of RORγt inhibitors. *J. Biol. Chem.* **2017**, *292* (28), 11618−11630.
(17) The Lilly Collection is routinely filtered for PAINS or otherwise promiscuous compounds. Bruns, R. F.; Watson, I. A. Rules for identifying potentially reactive or promiscuous compounds. *J. Med. Chem.* **2012**, *55* (22), 9763−9772.
(18) Jin, L.; Martynowski, D.; Zheng, S.; Wada, T.; Xie, W.; Li, Y. Structural basis for hydroxycholesterols as natural ligands of orphan nuclear receptor RORγ. *Mol. Endocrinol.* **2010**, *24* (5), 923−929.
(19) (a) The binding affinity of T0901317 in our hands was K_i = 310 nM. (b) Fauber, B. P.; de Leon Boenig, G.; Burton, B.; Eidenschenk, C.; Everett, C.; Gobbi, A.; Hymowitz, S. G.; Johnson, A. R.; Liimatta, M.; Lockey, P.; Norman, M.; Ouyang, W.; Rene, O.; Wong, H. Structure-based design of substituted hexafluoroisopropanol-arylsulfonamides as modulators of RORc. *Bioorg. Med. Chem. Lett.* **2013**, *23* (24), 6604−6609.
(20) Brzozowski, A. M.; Pike, A. C. W.; Dauter, Z.; Hubbard, R. E.; Bonn, T.; Engström, O.; Öhman, L.; Greene, G. L.; Gustafsson, J.-Å.; Carlquist, M. Molecular basis of agonism and antagonism in the oestrogen receptor. *Nature* **1997**, *389* (6652), 753−758.
(21) Fernández, A.; Berry, R. S. Extent of hydrogen-bond protection in folded proteins: a constraint on packing architectures. *Biophys. J.* **2002**, *83* (5), 2475−2481.
(22) Suzuki, S.; Nakamura, T.; Saito, R.; Terauchi, Y.; Kawai, K.; Takimoto-Kamimura, M.; Kurita, N. Structural change of retinoic-acid receptor-related orphan receptor induced by binding of inverse-agonist: molecular dynamics and ab initio molecular orbital simulations. *Comput. Struct. Biotechnol. J.* **2020**, *18*, 1676−1685.
(23) Pike, V. W.; Rash, K. S.; Chen, Z.; Pedregal, C.; Statnick, M. A.; Kimura, Y.; Hong, J.; Zoghbi, S. S.; Fujita, M.; Toledo, M. A.; Diaz, N.; Gackenheimer, S. L.; Tauscher, J. T.; Barth, V. N.; Innis, R. B. Synthesis and evaluation of radioligands for imaging brain nociceptin/orphanin FQ peptide (NOP) receptors with positron emission tomography. *J. Med. Chem.* **2011**, *54* (8), 2687−2700.
(24) Giuliano, C.; Jairaj, M.; Zafiu, C. M.; Laufer, R. Direct determination of unbound intrinsic drug clearance in the microsomal stability assay. *Drug Metab. Dispos.* **2005**, *33* (9), 1319−1324.
(25) We noted a general correlative trend but complex relationship between binding affinity and functional potency that has been described and explored by others in the nuclear receptor field; see for example: Jeyakumar, M.; Carlson, K. E.; Gunther, J. R.; Katzenellenbogen, J. A. Exploration of dimensions of estrogen potency parsing ligand binding and coactivator binding affinities. *J. Biol. Chem.* **2011**, *286* (15), 12971−12982.
(26) (a) Austin, R. P.; Barton, P.; Cockroft, S. L.; Wenlock, M. C.; Riley, R. J. The influence of nonspecific microsomal binding on apparent intrinsic clearance, and its prediction from physicochemical properties. *Drug Metab. Dispos.* **2002**, *30* (12), 1497−1503. (b) Liu, X.; Wright, M.; Hop, C. E. C. A. Rational use of plasma protein and tissue binding data in drug design. *J. Med. Chem.* **2014**, *57* (20), 8238−8248.
(27) (a) Schubert, D.; Maier, B.; Morawietz, L.; Krenn, V.; Kamradt, T. Immunization with Glucose-6-Phosphate Isomerase Induces T Cell-Dependent Peripheral Polyarthritis in Genetically Unaltered Mice. *J. Immunol.* **2004**, *172* (7), 4503−4509. (b) Matsumoto, I.; Zhang, H.; Yasukochi, T.; Iwanami, K.; Tanaka, Y.; Inoue, A.; Goto, D.; Ito, S.; Tsutsumi, A.; Sumida, T. Therapeutic effects of antibodies to tumor necrosis factor-α, interleukin-6 and cytotoxic T-lymphocyte antigen 4 immunoglobulin in mice with glucose-6-phosphate isomerase induced arthritis. *Arthritis Res. Ther* **2008**, *10* (3), R66.
(28) (a) Iwanami, K.; Matsumoto, I.; Tanaka, Y.; Inoue, A.; Goto, D.; Ito, S.; Tsutsumi, A.; Sumida, T. Arthritogenic T cell epitope in glucose-6-phosphate isomerase-induced arthritis. *Arthritis Res. Ther* **2008**, *10* (6), R130. (b) Iwanami, K.; Matsumoto, I.; Tanaka-Watanabe, Y.; Inoue, A.; Mihara, M.; Ohsugi, Y.; Mamura, M.; Goto, D.; Ito, S.; Tsutsumi, A.; Kishimoto, T.; Sumida, T. crucial role of the interleukin-6/interleukin-17 cytokine axis in the induction of arthritis by glucose-6-phosphate isomerase. *Arthritis Rheum.* **2008**, *58* (3), 754−763.
(29) Langley, R. G.; Elewski, B. E.; Lebwohl, M.; Reich, K.; Griffiths, C. E. M.; Papp, K.; Puig, L.; Nakagawa, H.; Spelman, L.; Sigurgeirsson, B.; Rivas, E.; Tsai, T.-F.; Wasel, N.; Tyring, S.; Salko, T.; Hampele, I.; Notter, M.; Karpov, A.; Helou, S.; Papavassilis, C. Secukinumab in plaque psoriasis results of two phase 3 trials. *N. Engl. J. Med.* **2014**, *371* (4), 326−338.
(30) Gordon, K. B.; Blauvelt, A.; Papp, K. A.; Langley, R. G.; Luger, T.; Ohtsuki, M.; Reich, K.; Amato, D.; Ball, S. G.; Braun, D. K.; Cameron, G. S.; Erickson, J.; Konrad, R. J.; Muram, T. M.; Nickoloff, B. J.; Osuntokun, O. O.; Secrest, R. J.; Zhao, F.; Mallbris, L.; Leonardi, C. L. Phase 3 trials of ixekizumab in moderate-to-severe plaque psoriasis. *N. Engl. J. Med.* **2016**, *375* (4), 345−356.
(31) (a) Grime, K.; Riley, R. The impact of in vitro binding on in vitro - in vivo extrapolations, projections of metabolic clearance and clinical drug-drug interactions. *Curr. Drug Metab.* **2006**, *7* (3), 251−264. (b) Riley, R. J.; McGinnity, D. F.; Austin, R. P. A unified model for predicting human hepatic, metabolic clearance from in vitro intrinsic clearance data in hepatocytes and microsomes. *Drug Metab. Dispos.* **2005**, *33* (9), 1304−1311.
(32) Øie, S.; Tozer, T. N. Effect of altered plasma protein binding on apparent volume of distribution. *J. Pharm. Sci.* **1979**, *68* (9), 1203−1205.
(33) Bockermann, R.; Schubert, D.; Kamradt, T.; Holmdahl, R. Induction of a B-cell-dependent chronic arthritis with glucose-6-phosphate isomerase. *Arthritis Res. Ther* **2005**, *7* (6), R1316.
(34) Patel, N. J.; Wickremsinhe, E.; Hui, Y.-H.; Barr, A.; Masterson, N.; Ruterbories, K.; Weller, J.; Hanes, J.; Kern, T.; Perkins, E. Evaluation and optimization of blood micro-sampling methods: serial sampling in a cross-over design from an individual mouse. *J. Pharm. Pharm. Sci.* **2016**, *19* (4), 496−510.

NOTE ADDED AFTER ASAP PUBLICATION

This paper was published ASAP on April 14, 2021, with errors in the TOC/abstract graphic. The updated version was reposted on April 16, 2021.

https://doi.org/10.1021/acs.jmedchem.0c01918
J. Med. Chem. 2021, 64, 5470−5484